Chirality sensing employing parity-time-symmetric and other resonant gain-loss optical systems

Ioannis Katsantonis [1,2,*] Sotiris Droulias,[1,3] Costas M. Soukoulis,[1,4] Eleftherios N. Economou,[1,5]
T. Peter Rakitzis [1,5] and Maria Kafesaki [1,2,†]

[1]*Institute of Electronic Structure and Laser, Foundation of Research and Technology Hellas, 71110 Heraklion, Crete, Greece*
[2]*University of Crete, Department of Material Science and Technology, 71003 Heraklion, Greece*
[3]*Department of Digital Systems, University of Piraeus, Piraeus 18534, Greece*
[4]*Ames Laboratory and Department of Physics and Astronomy, Iowa State University, Ames, Iowa 50010, USA*
[5]*University of Crete, Department of Physics, 71003 Heraklion, Greece*

Molecular chirality detection and enantiomer discrimination are very important issues for many areas of science and technology, prompting intensive investigations via optical methods. However, these methods are hindered by the intrinsically weak nature of chiro-optical signals. Here, we investigate and demonstrate the potential of gain materials and of combined gain-loss media to enhance these signals. Specifically, we show that the proper combination of a thin chiral layer with a gain-loss bilayer can lead to large enhancements of both the circular dichroism (CD) response and the dissymmetry factor *g* compared with the chiral layer alone. The most pronounced enhancements are obtained in the case of a parity-time (*PT*) symmetric gain-loss bilayer, while deviations from the exact *PT* symmetry lead to only moderate changes of the CD and *g* response, demonstrating also the possibility of tuning the system response by tuning the gain layer properties. In the case of *PT*-symmetric gain-loss bilayers, we found that the largest CD enhancement is obtained at the system lasing threshold, while the *g* enhancements are at the anisotropic transmission resonances of the systems. Our results clearly demonstrate the potential of gain materials in chirality detection. Moreover, our gain-involving approach can be applied in conjunction with most of the nanophotonics/nanostructures-based approaches that have already been proposed for chirality sensing, further enhancing the performance/output of both approaches.

I. INTRODUCTION

Chiral objects, i.e., three-dimensional objects that present mirror asymmetry [1], are all around us, ranging from our DNA and other important biomolecules to chemical drugs, and extending over spiral galaxies [2]. Chiral objects are classified according to their handedness, with the left- and right-handed forms of an object known as enantiomers. There are many chiral biomolecules and chemical drugs for which the two enantiomers interact differently with a biological organism having severely different therapeutic and/or toxicological effects [3]. Therefore, an efficient detection and discrimination of the different enantiomers of a chiral substance is crucially important in many scientific fields, like medicine, pharmacology, biology, chemistry [4], and fundamental physics [5]. A major problem, though, in this detection is the very weak chiro-optical signals encountered in all the light-related schemes applied for chirality detection.

Chirality, in addition to being a property of matter, is a property of the electromagnetic field [6]. Although the electromagnetic field cannot be chiral in the conventional sense, as it is not an object, the chirality arises from the polarization rotating electric and magnetic fields as the wave propagates in space, forming left- or right-handed helical patterns. The field chirality is usually quantified by the quantity $C = -\omega \text{Im}[\mathbf{E} \cdot \mathbf{H}^*]/2c^2$, proportional to the inner product of electric and magnetic field, which is called optical chirality [6,7] (ω is the wave frequency and c the vacuum light speed). The simplest example of a chiral field is circularly polarized (CP) light, and it has been used for over 200 years to measure molecular chirality [8]. Fields of higher C than CP light are characterized as superchiral. Recent studies have shown that superchiral fields can play an important role in the detection of chiral molecules, as they offer enhancement of chiro-optical signals, thus greatly facilitating the chirality detection and the discrimination of the different enantiomers [6]. Therefore, many studies have been devoted recently to the generation of strong superchiral fields and their exploitation for chiral molecule detection [7,9–21]. Many of them have explored various nanophotonic [10], plasmonic [11,12], and metamaterial platforms [15] as means to enhance chiral local fields. For example, high-index dielectric nanoparticles [10,14,16–18], plasmonic spheres [9] or disks [10], helicity preserving optical cavities [13,19,20,22–24], and others [16,25–27] have been employed for chiral detection and enhancement of chiral sensing. However, all the above-mentioned approaches target enhancement of the circular dichroism (CD) response signal [i.e., the absorption difference between right-handed CP (RCP/+) and left-handed CP (LCP/−) incident waves, i.e., $A_+ - A_-$], a quantity directly proportional to the volume of the chiral substance to be detected. A quantity strongly related to CD, of additional merit regarding chiral interactions

*katsantonis@iesl.forth.gr
†kafesaki@iesl.forth.gr

and chirality sensing, is the so-called Kuhn's dissymmetry factor g [7,18,28–30], defined as the absorption difference for RCP and LCP waves (i.e., the CD) divided by the average absorption [i.e., $(A_+ + A_-)/2$]:

$$g = \frac{(A_+ - A_-)}{(A_+ + A_-)/2} \propto \frac{8c\kappa''C}{\omega(\varepsilon''|\mathbf{E}|^2 + \mu''|\mathbf{H}|^2)}. \quad (1)$$

In Eq. (1), C is the optical chirality (see Appendix F for details), and ε'', μ'', and κ'' are the imaginary part of electric permittivity, magnetic permeability and chirality parameter, respectively, of the chiral medium. [For the derivation of the right-hand side of Eq. (1), see Appendix F.]

The dissymmetry factor g is a useful dimensionless quantity describing the relative preferential absorption of CP waves by a chiral sample. Enhanced g results to enhanced enantioselectivity in all chiral light-matter interactions involving light absorption, including fluorescence (used, e.g., for sensing [7], photolysis, and photopolymerization [4]). From Eq. (1), it is evident that the relative chiral asymmetry in the absorption is proportional to both the chirality of matter (κ) and the chirality of the electromagnetic field (C); therefore, its maximization through proper electromagnetic field enhancement or structuring promises a viable route toward enhanced enantioselectivity in chiral light-matter interactions. Maximization of g using common nanophotonic resonances and platforms [7,26,31,32] is not a straightforward task, as the maximization of the absorption difference there (numerator of g) is always associated with enhancement of the absolute absorptions A_+ and A_- (g denominator), which reduces the g value. Approaches to enhance g, in addition to the change/optimization of the nanophotonic or metamaterial structure employed, include optical approaches to create superchiral light. The dominant approach is the exploitation of field nodes created in a cavity by the interference of two counterpropagating CP waves [7], while other approaches include an efficient manipulation of the orbital angular momentum delivered by optical vortices [33] and the use of nonlinear phenomena [34]. However, most of the above-mentioned approaches, especially the first one, are associated with small field intensities in the region of the superchiral fields, thus limiting the overall efficiency of the light-matter interaction.

A simple approach that can decouple the simultaneous maximization of the numerator and denominator of g, being thus suitable for its maximization without concurrent minimization of the overall field intensity, can be offered by the involvement of gain media. Here, we propose and investigate such an approach and its potential and capabilities for CD and dissymmetry factor enhancement in a molecular chirality sensing scheme. We propose a simple structure combining a thin chiral layer (which is the chiral material under detection) with gain and loss media in balance, as to exhibit parity-time (*PT*) symmetry, or beyond such a balance. *PT*-symmetric systems exploit strong electromagnetic fields at the interfaces of the gain-loss media [35,36] as well as exotic scattering features, such as anisotropic transmission resonances (ATRs) [35], and exceptional points associated with strong sensitivity [37–40]. Due to such peculiar features, *PT*-symmetric optical systems have gained growing attention in both fundamental and applied research [41–53].
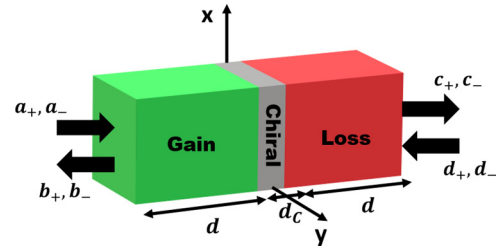

FIG. 1. A three-layer system, consisting of a thin layer of a chiral medium sandwiched between a gain and a loss slab (both of thickness d along the z direction and infinite along x and y). $a_\pm$, $b_\pm$, $c_\pm$, and $d_\pm$ are the amplitudes of ingoing and outgoing (see arrows) right-handed circularly polarized (RCP/+) and left-handed circularly polarized (LCP/−) waves.

As already mentioned, there are many works investigating and proposing schemes for efficient molecular chirality detection and enantiomer discrimination. Since chiral light-matter interactions are inherently extremely weak (at optical frequencies, natural materials have $\kappa \sim 10^{-5}$), this detection can be very challenging, especially when only tiny amounts of substances are involved, e.g., ultrathin chiral layers. We show here that our approach of combining a thin chiral layer with a gain-loss *PT*-symmetric bilayer can to a large degree overcome the main challenges involved in chiral detection. More specifically, by both analytical and numerical calculations, we demonstrate strong CD signals in our *PT*-symmetric system and high values of the dissymmetry factor g. Furthermore, we investigate the necessity of the *PT*-balanced gain-loss in our system; by changing the gain-loss ratio, we can still achieve enhanced CD and dissymmetry factor, while overcoming the strict *PT*-symmetry highly facilitates experimental realization and validation of our findings. Investigating further the origin and the potential of the g enhancement in our systems, we find that (a) in *PT*-symmetric systems, it occurs at the ATR points of the systems [35], which are associated with unidirectional zero reflection and unity transmission; and (b) g enhancement is associated with no reduction or even enhancement of the total field intensity, a quantity critical for the overall efficiency of any light-matter interaction. Finally, we must mention that our approach of employing gain media for chirality sensing can be used in conjunction with most of the proposed nanophotonics-based approaches, expanding further their potential as chirality sensing platforms and proposing the area of active nanophotonics as a viable route for chirality sensing and differentiation.

II. *PT*-SYMMETRIC TRILAYERS

In this paper, we first consider a three-layer geometry with total thickness $L = d + d_C + d$ along the z direction (and infinite along the x and y directions) in free space, as shown in Fig. 1, where a thin chiral layer, of thickness d_C, is sandwiched between a gain and a loss layer, both of thickness d. We use the $\exp(-i\omega t)$ time convention (in this convention, the positive imaginary part of the refractive index describes loss, while negative values of this quantity correspond to gain).

We are interested in exploiting the electromagnetic response of our purposed system under CP incident

waves. We solve Maxwell's equations $\nabla \times \mathbf{E} = i\omega\mathbf{B}$ and $\nabla \times \mathbf{H} = -i\omega\mathbf{D}$ with the appropriate boundary conditions, and for the chiral layer, we assume the constitutive relations [54] $\mathbf{D} = \varepsilon_r\varepsilon_0\mathbf{E} + i(\kappa/c)\mathbf{H}$ and $\mathbf{B} = \mu_r\mu_0\mathbf{H} - i(\kappa/c)\mathbf{E}$, where ε_r, μ_r, and κ refer to the relative permittivity, permeability, and the chirality (Pasteur) parameter (quantifying the magnetoelectric coupling), respectively (ε_0 and μ_0 are the vacuum permittivity and permeability, respectively). Inserting the above constitutive relations into Maxwell's equations, we can find the chiral Helmholtz equation to be $\nabla^2\mathbf{E} + \omega^2[\frac{(\varepsilon_r\mu_r - \kappa^2)}{c^2}]\mathbf{E} + (\frac{2\omega\kappa}{c^2})\nabla \times \mathbf{E} = 0$. Assuming plane waves propagating along z, we obtain the elementary solutions of the chiral Helmholtz equation as $\mathbf{E}_\pm = E_\pm(\hat{\mathbf{x}} \pm i\hat{\mathbf{y}})\exp[i(k_\pm z - \omega t)]$, where $k_\pm = \omega(\sqrt{\varepsilon_r\mu_r} \pm \kappa)/c$ are the wave vectors in the chiral slab, and E_+ and E_- are the amplitudes for RCP and LCP waves, respectively (employing source side view). The magnetic field can be found from $\mathbf{E}_\pm$ by $\mathbf{H}_\pm = \mp iZ^{-1}\mathbf{E}_\pm$, where $Z = \sqrt{\frac{\mu_r\mu_0}{\varepsilon_r\varepsilon_0}}$ is the wave impedance.

For the (nonchiral) gain and loss media, the above equations are simplified by taking $\kappa = 0$, so the wave vector takes the well-known form $k = \frac{\omega}{c}\sqrt{\varepsilon_r\mu_r}$. To obtain general expressions allowing investigation of different material combinations, we start with layers of arbitrary material parameters. Considering incident LCP and RCP waves and requiring the continuity of the tangential components (x, y) of $\mathbf{E}$ and $\mathbf{H}$ at each of the four interfaces of the system $[z = -(d + \frac{d_C}{2}), \ z = -\frac{d_C}{2}, \ z = \frac{d_C}{2}, \text{ and } z = (d + \frac{d_C}{2})]$, we obtain a 16×16 linear system of equations which is solved analytically, giving the scattering coefficients (transmission and reflection) of the total system (see Appendix A for analytical expressions).

III. CIRCULAR DICHROISM RESPONSE

To characterize the chiral response of our system, and through it the chiral properties of the chiral layer under investigation, we further analyze the scattering properties, calculating CD $= A_+ - A_-$. The absorption coefficients are given by $A_+ = 1 - |t_{++}|^2 - |r_{-+}|^2$ for RCP/+ and $A_- = 1 - |t_{--}|^2 - |r_{+-}|^2$ for LCP/− incidence, where the first subscript in the transmission (t) and reflection (r) coefficients indicates the output polarization and the second the incident polarization. The different subscripts in the reflection coefficients are due to the property of chiral interfaces to reverse the circular polarization upon reflection [55,56], i.e., when an incidence wave is RCP, it is transformed to LCP upon reflection and vice versa. By analytical calculations, we find $r_{-+} = r_{+-}$ for incidence from either side of the system; hence, the CD is proportional to the transmission difference for LCP and RCP waves, and it is the same for left- and right-side incident waves due to reciprocity. Calculating the CD for the case of PT-symmetric loss and gain slabs, i.e., with equal real parts of permittivity and permeability and opposite imaginary parts [35–38,41,42], we find

$$\text{CD} = |t_{--}|^2 - |t_{++}|^2 = \frac{512\exp(-2kd_C\text{Im}[n_C])}{|Z_G Z_C Z_L \ (A_1 + A_2 + B_1 + B_2)|^2}$$
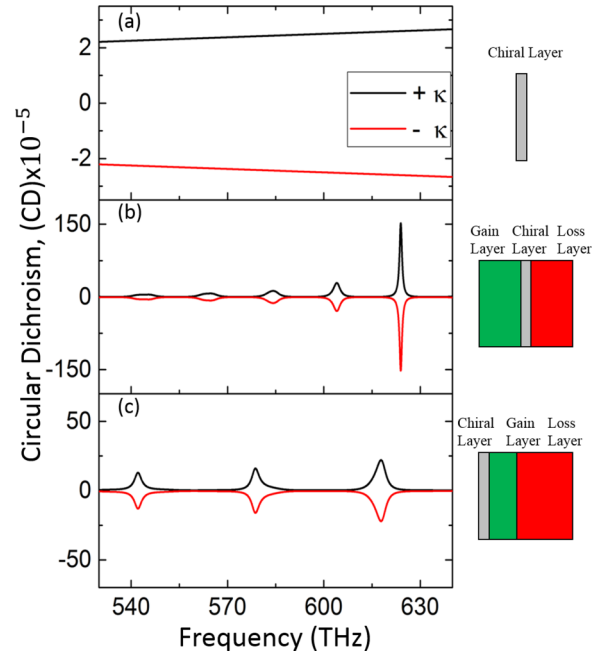$$\times \sinh(2kd_C\text{Im}[\kappa]), \qquad (2)$$

FIG. 2. Circular dichroism (CD) for the system shown in Fig. 1 and two related systems. (a) corresponds to a chiral layer alone; (b) corresponds to the PT-symmetric system shown in Fig. 1 with the middle/chiral layer the same as in (a); and (c) corresponds to a general non-Hermitian system, again with the same chiral layer (gray area) but placed next to the gain layer. For geometrical and material parameters, see main text. The black lines correspond to positive sign of the chirality (both real and imaginary) κ of the chiral layer and the red lines to negative sign. The transmission amplitudes employed for the CD calculation as well as the CD in a broader frequency region are shown in Fig. 8 in Appendix D.

where $k = \omega/c$ is the wave number in the vacuum, and $n_C = \sqrt{\varepsilon_C\mu_C}$ is the nonchiral part of the index of refraction in the chiral medium. The wave impedance in each layer is $Z_i = \sqrt{\mu_0\mu_i/\varepsilon_0\varepsilon_i}$, where the subscript $i = \{G, C, L\}$ denotes the gain, chiral, or loss region, respectively. The terms A_1, A_2 and B_1, B_2 in Eq. (2) depend on the impedances and wave vectors and are totally independent of the chirality parameter κ (see Appendixes A and B). Thus, Eq. (2) shows that CD depends only on the imaginary part of the chirality parameter [through $\sinh(2kd_C\text{Im}[\kappa])$]; for positive chirality, $\text{Im}[\kappa] > 0$, the hyperbolic sin is positive, while for negative chirality, $\text{Im}[\kappa] < 0$, sinh is negative; this change of sign allows employment of the system for discrimination of the two different enantiomers of a chiral molecular system (note that the two enantiomers have opposite chirality parameter κ). The sinh prefactor in Eq. (2) depends only on the nonchiral absorption of the chiral layer (via $\text{Im}[n_c]$) as well as on the gain-loss media and determines the position of the resonances of the total system.

In the following, we apply our formalism to systems with close-to-realistic material parameters to investigate and quantify the potential of those systems for molecular chirality sensing. In Fig. 2(a), we plot the CD for a thin chiral layer alone (of thickness $d_C = 10\,\text{nm}$), with chirality parameter $\kappa = \pm 5(10^{-4} + 10^{-5}i)$, which is very close to the chirality of

aqueous solutions of chiral molecules [22] and with a typical ratio between real and imaginary parts [57]; its nonchiral refractive index is $n_C = 1.33 + 0.01i$. In Fig. 2(b), we plot the CD for the thin chiral slab placed in the middle of a *PT*-symmetric bilayer, as shown in Fig. 1 (see also Fig. 8 in Appendix D for the CD in a wider frequency range). The gain and loss slabs have refractive index $n_{G/L} = 3 \mp 0.04i$, where the − sign corresponds to the gain medium and the + sign to the loss medium, as dictated by *PT* symmetry [48]. (Note that *PT*-symmetric optical systems with parameters very close to ours have already been studied both theoretically [48] and experimentally [58,59]. Note also that the gain value employed, although not achievable with the current bulk gain materials, can be achieved (as effective gain) in gain-involving metamaterials, due to the resonance-induced enhancement. Each of the two layers has thickness $d = 2.5 \ \mu$m. The black lines in Fig. 2 correspond to positive signs in the chirality parameter and the red lines to negative signs. We observe that the CD depends on the sign of the imaginary part of chirality, as predicted from Eq. (2). Comparing Figs. 2(a) and 2(b), we observe that the presence of the *PT*-symmetric bilayer leads to CD up to 75× larger than that of the chiral layer alone. As a comparison, we note that the CD signal of our *PT*-symmetric configuration is close to one order of magnitude larger than the CD signals of the chiral and achiral nanophotonic systems that have been already studied and proposed for chirality sensing [9].

Because of the strict conditions imposed by the full *PT*-symmetry requirement, which limit the practical realization and exploitation of such systems, it is important to know if and to what extent the exact *PT*-symmetry condition is essential for the observed CD enhancement. For that, we investigated also general non-Hermitian systems where the gain-loss media are not in balance. An example is shown in Fig. 2(c) (see also Fig. 8 in Appendix D), where we assume a gain layer with index $n_G = 2 - 0.05i$ and thickness $d_G = 2 \ \mu$m, a loss layer with index $n_L = 3 + 0.04i$ and thickness $d_L = 3 \ \mu$m, and where the chiral layer [same as in Figs. 2(a) and 2(b)] is placed at the left side of the gain-loss bilayer (i.e., it is attached to the gain layer); this configuration is more amenable to experimental realization. We observe also here a CD enhancement comparable with Fig. 2(b), despite the thinner-gain and thicker-loss layer. We observe that, at frequencies ∼617 THz, we have values of CD >10 times larger than that of the chiral layer alone. The large CD enhancement regions in both cases of Figs. 2(b) and 2(c) coincide with the transmission resonances of the structures (Fabry-Perot resonances; see Fig. 8 in Appendix D), while the largest enhancement is obtained at frequencies 643.7 and 655 THz, respectively, which are close to the lasing threshold of the corresponding structure [35]—see Fig. 8 in Appendix D.

Note that the CD peaks of both systems of Fig. 2 are associated with quite high quality factor ($Q = \frac{\text{Re}[\omega_0]}{2\text{Im}[\omega_0]} > 100$, where ω_0 is the resonance frequency), not only around the lasing threshold but also below the lasing threshold (and exceptional point). This is attributed to the balanced gain-loss, particularly in the *PT*-symmetric case. In *PT* systems, below the exceptional point, the gain balances the loss [35–38,41–50], and we have almost lossless modes. As the frequency increases and the system approaches the lasing threshold, a
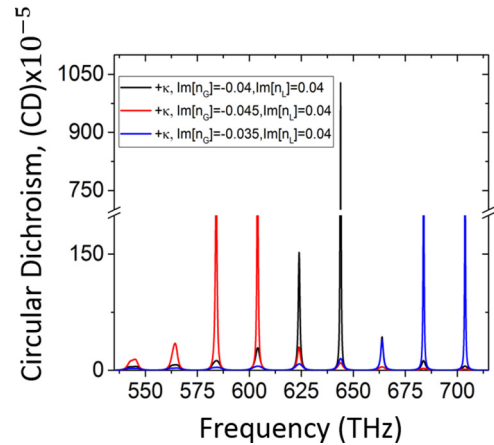

FIG. 3. Circular dichroism (CD) three different gain-loss [Im(n_G)-Im(n_L)] ratios for the system of Fig. 2(b). In all cases, we assume positive sign of the chirality parameter (both real and imaginary parts) of the thin chiral layer.

transmission pole in the complex frequency plane approaches and finally crosses the real axis, i.e., $\text{Im}[\omega_0] \to 0 \Rightarrow Q \to \infty$.

To investigate further and understand the role and necessity of *PT* symmetry regarding the achievable CD enhancement, we calculated the CD for the system of Fig. 1 for different gain-loss contrasts. The result is shown in Fig. 3 and compared with the exact *PT* case (the one of Figs. 2(b) and 8 in Appendix D). As can be seen in Fig. 3, a small deviation (increase/decrease of gain) from the exact *PT*-symmetric case (black line in Fig. 3) leads to only moderate deterioration of the CD peaks. Moreover, with increase of the gain parameter [Im(n_G)], we observe a frequency shift in the maximum CD response due to the lasing threshold and the corresponding exceptional point moving in lower frequencies [35], while the opposite behavior is observed with decrease of the gain parameter. We must note here that, when the system reaches the lasing threshold, it becomes unstable (a self-sustained oscillator); hence, quantities such as transmittance power are not well defined. That is why we concentrate our attention mostly before the lasing threshold, where strong CD enhancement also takes place. The results of Fig. 3 clearly demonstrate that *PT*-symmetric gain-loss is a sufficient but not a necessary condition for large CD enhancement in gain-loss systems.

IV. DISSYMMETRY FACTOR

As already mentioned in the introduction, the dissymmetry factor determines to a large degree the percentage of enantioselectivity in all photoinduced chiral light-matter interactions (photoionization, fluorescence, photolysis, etc.), which can be exploited not only for enantiomer discrimination but also for enantioselective synthesis, critical for the pharmaceutical industry. To evaluate the dissymmetry factor in our system, we employ the defining Eq. (1); there we notice that the numerator CD [see Eq. (2)] depends on the chirality as $\sinh(2kd_C\text{Im}[\kappa])$, and it is independent of the side of incidence. The total absorption [denominator of Eq. (1)], $A_+ + A_- = 2 - |t_{++}|^2 - |t_{--}|^2 - |r_{-+}|^2 - |r_{+-}|^2$, depends on the reflection which is different for waves incident from opposite
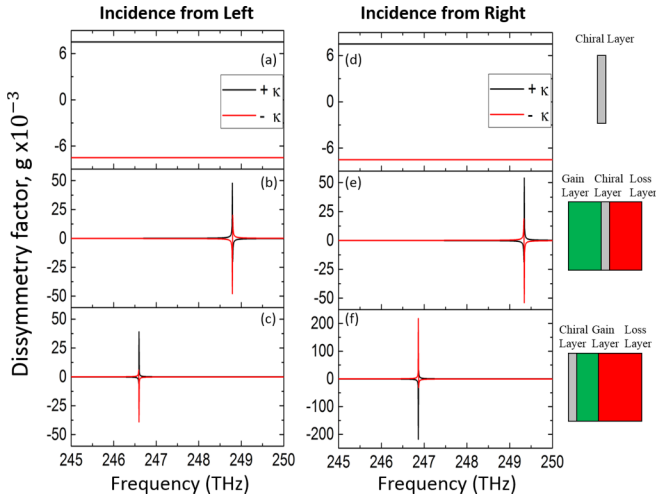
FIG. 4. Dissymmetry factor g calculations for the three systems of Fig 2, with waves incident from the left side (left column) and waves incident from the right side (right column) of the systems; (a) and (d) correspond to the chiral layer alone, (b) and (e) correspond to the PT-symmetric system, and (c) and (f) to the general non-Hermitian system. The black lines correspond to positive sign of the chirality (both real and imaginary) κ of the chiral layer and the red lines to negative sign. The material parameters are the same as in Fig. 2.

system sides, making the dissymmetry factor side dependent. From analytical calculations, we find for the system of PT-symmetric gain-loss layers the dissymmetry factor for waves incident from the left $g^{(L)}$ and from the right $g^{(R)}$ as

$$g^{(L)} = -2\tanh(2kd_C\mathrm{Im}[\kappa]) + 512\exp(-2kd_C\mathrm{Im}[n_C])$$
$$\times \sinh(2kd_C\mathrm{Im}[\kappa])\left[\frac{1}{P} + \frac{1}{Q^{(L)}}\right], \quad (3)$$

$$g^{(R)} = -2\tanh(2kd_C\mathrm{Im}[\kappa]) + 512\exp(-2kd_C\mathrm{Im}[n_C])$$
$$\times \sinh(2kd_C\mathrm{Im}[\kappa])\left[\frac{1}{P} + \frac{1}{Q^{(R)}}\right], \quad (4)$$

where $P = |Z_G Z_C Z_L (A_1 + A_2 + B_1 + B_2)|^2$, $Q^{(L)} = |Z_G Z_C Z_L [C_1^{(L)} + C_2^{(L)} + D_1^{(L)} + D_2^{(L)}]|^2$, and $Q^{(R)} = |Z_G Z_C Z_L [C_1^{(R)} + C_2^{(R)} + D_1^{(R)} + D_2^{(R)}]|^2$. The terms $C_1^{(R)}$, $C_2^{(R)}$, $D_1^{(R)}$, and $D_2^{(R)}$ in $Q^{(R)}$ and $C_1^{(L)}$, $C_2^{(L)}$, $D_1^{(L)}$, and $D_2^{(L)}$ in $Q^{(L)}$ are given in Appendix A.

To obtain quantitative data regarding the dissymmetry factor, we consider the same systems as in Fig. 2. In Fig. 4, we plot the dissymmetry factor g for CP waves impinging our systems from both sides. In panels (a) and (d), we show the g values for the chiral layer alone (for comparison); it is evident that g depends on the sign of chirality [through the CD numerator of Eq. (1)]. In panels (b) and (e), we present the g values for the PT-symmetric case. We observe two discrete side-dependent peaks which demonstrate an up to $7\times$ g enhancement compared with the chiral layer alone. The positions of the peaks are at frequencies where the total absorption [denominator of Eq. (1)] approaches zero (but not exactly zero, where g goes to infinity), as we will discuss and analyze in more detail later on. Finally, in panels (c)

and (f), we observe, like the PT-symmetric case, behavior in the more general non-Hermitian system of unbalanced loss and gain materials [system of Fig. 2(c)]. Again here, the g peaks are observed at frequencies where the total absorption (denominator of g) tends to zero. (Note that, although the term *absorption* is usually connected with material losses and takes positive values, here, we keep the same terminology even for materials with gain, meaning field enhancement and taking negative values.) Observing the results of Fig. 4, one can also see an asymmetry in the g-resonance profile, resembling antisymmetric Fano profiles, like the ones discussed in Ref. [60]. This asymmetry seems to originate from the asymmetric coupling of the chiral layer with the gain and loss layers as well as from the asymmetry of the propagation (and absorption) characteristics for left and right incidence, as is revealed from the corresponding field analysis (see Sec. VI).

V. SCATTERING MATRIX ANALYSIS OF THE PT-TRILAYER STRUCTURE

To fully understand the response of our non-Hermitian three-layer structures and the origin of the high achievable g values, we further investigate the scattering properties of our systems. Scattering processes are usually characterized by the properties (eigenvalues, eigenvectors, poles, zeros, etc.) of the scattering matrix S, which describes the relation between incoming and outgoing waves [35,49–53]. In our scattering (reflection/transmission) system, depending on the arrangement of the input and output ports (RCP or LCP waves), we can build our scattering matrix formalism in several ways. However, there are two cases/arrangements, which characterize two different physical processes. The first case, called here $S^{(1)}$, is related to the position of exceptional points, at which the system passes from PT-symmetric phase (associated with real spectrum and PT-symmetric eigenfunctions) to broken-PT phase [35] (complex spectrum, non-PT-symmetric eigenfunctions), i.e., the points at which the scattering matrix eigenvalues cease to be unimodular are the exceptional points, marking the change of the PT phase. In the second scattering matrix case, called here $S^{(2)}$, the points at which the scattering matrix eigenvalues cease to be unimodular (called here crossing points) correspond to ATRs, in which the reflection from one side (left or right) vanishes, and the transmission is unity [35], leading to zero absorption, a condition favoring dissymmetry factor enhancement. This second S-matrix configuration has already been discussed quite extensively in the case of nonchiral PT-symmetric systems [19,44] (2×2 scattering matrix). In the case of systems involving chiral media, because of the two possible input/circular polarizations at each of the two sides of the structure, the system needs to be described by a 4×4 scattering matrix $S^{(2)}$ [50–52]. Here, $S^{(2)}$ is defined by

$$\begin{pmatrix} c_+ \\ b_- \\ c_- \\ b_+ \end{pmatrix} = S^{(2)} \begin{pmatrix} a_+ \\ d_- \\ a_- \\ d_+ \end{pmatrix} \equiv \begin{pmatrix} t_{++}^{(L)} & r_{+-}^{(R)} & 0 & 0 \\ r_{-+}^{(L)} & t_{--}^{(R)} & 0 & 0 \\ 0 & 0 & t_{--}^{(L)} & r_{-+}^{(R)} \\ 0 & 0 & r_{+-}^{(L)} & t_{++}^{(R)} \end{pmatrix} \begin{pmatrix} a_+ \\ d_- \\ a_- \\ d_+ \end{pmatrix},$$
$$(5)$$

where the input and output wave amplitudes are shown in Fig. 1. The calculation of the eigenvalues of $S^{(2)}$ yields two
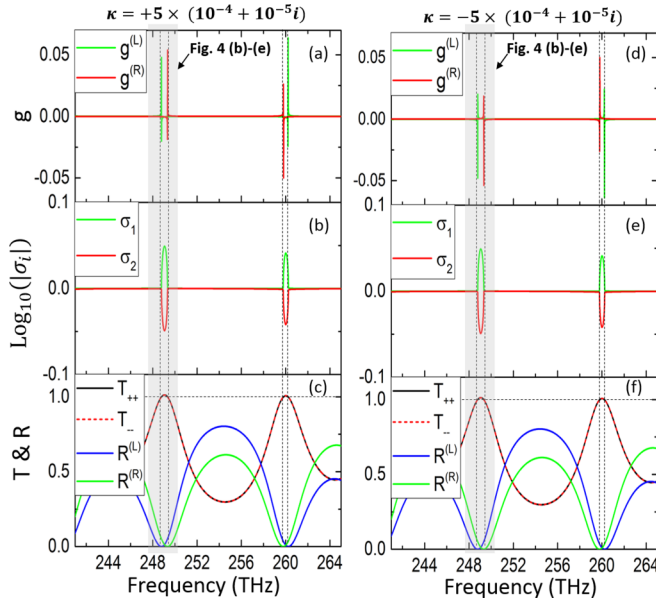
FIG. 5. (a) and (d) Dissymmetry factor calculations for the system of Figs. 4(b) and 4(e), with positive (left column) and negative (right column) chirality parameter. (b) and (e) Eigenvalues of the scattering matrix $S^{(2)}$. (c) and (f) Transmission and reflection power coefficients for circularly polarized plane waves impinging in both sides of the system. The vertical dashed lines correspond to the anisotropic transmission resonances (ATRs) of the system.

degenerate pairs of eigenvalues, which are given by

$$\sigma_{1,2} = \tfrac{1}{2}[t_{++} + t_{--} \pm \sqrt{(t_{--} - t_{++})^2 + 4r^{(L)}r^{(R)}}] \qquad (6)$$

Figures 5(b) and 5(e) show the eigenvalues of $S^{(2)}$ for our *PT*-symmetric case [system of Fig. 4(b)]. Although these eigenvalues depend on the chiral layer chirality, here, due to the small thickness of the chiral layer (10 nm) and the very weak chiral response (of the order of 10^{-5}), the chiral dependence can be assumed as a small perturbation; thus, the eigenvalues are practically independent of chirality. If the chirality parameter is strong, i.e., in chiral metamaterials [56], the non-Hermitian/*PT*-symmetric properties, like exceptional points and ATRs, are strongly dependent and controllable by the chirality [51]. As can be seen in Fig. 5, at the transition points from unimodular to nonunimodular eigenvalues (multiple points in this case), which coincide with the ATRs [35], the reflection from one system side is zero, while both transmittances approach unity ($T_{++} = |t_{++}|^2 \cong 1$ and $T_{--} = |t_{--}|^2 \cong 1$)—see Figs. 5(c) and 5(f). Considering the above properties, the total absorption goes to zero, $A_+ + A_- = 2 - T_{++} - T_{--} \cong 0$; this quantity is displayed in the denominator of the dissymmetry factor g [Eq. (1)]; hence, the points where a g peak occurs in our *PT*-symmetric system coincide with the ATR points of the system, as shown comparing Figs. 5(a) and 5(d) with Figs. 5(b) and 5(e), respectively. These figures clearly demonstrate and highlight the importance of the ATR points of *PT*-symmetric systems for g-factor maximization. Note that the results shown in Fig. 5 concern only a relatively narrow frequency region; analogous results for a much broader frequency range are shown in Fig. 8 in Appendix D.

Those results demonstrate a multitude of frequency ranges where g enhancement is achievable, both above and below the system exceptional point—for the *PT*-like case.

VI. FIELD ANALYSIS AND DISCUSSION

As was mentioned also in the introduction and in the previous section, the interplay between loss and gain media (resulting in positive and negative absorption, respectively) allows vanishing of the total absorption without reduction of the field intensity in the system. Thus, in principle, one has the potential to enhance the dissymmetry factor, enhancing thus the enantioselectivity of the chiral light-matter interaction, keeping also high field intensity values, i.e., keeping or enhancing the overall efficiency of the interaction. To demonstrate this potential for our systems, we evaluate and plot the electric field intensity and the field chirality C along the system for the systems shown in Figs. 2 and 4 at the frequencies of the evaluated g peaks shown in Fig. 4. For completeness and comparison, we present the same quantities also at CD peaks. The results are shown in Fig. 6.

More specifically, in Figs. 6(a) and 6(c), we plot the normalized electric field along the *PT*-symmetric trilayer structure, as well as the optical chirality (normalized by the vacuum optical chirality C_0—note that the field is everywhere in our system CP) for RCP wave propagation, at frequency 248.79 THz for waves incident from the left side [Fig. 6(a)] and at frequency 249.34 THz for waves incident from the right side [Fig. 6(c)]. (Note that these frequencies coincide with the g peaks of Figs. 4(b) and 4(e) and that very similar results are obtained also for LCP waves—not shown here.) We observe that both the field intensity and the optical chirality are enhanced toward the center of the system (where the chiral layer is located) when the wave incidence is from the gain side, while they decrease for incidence from the loss side, even though the transmission and reflection is in both cases the same. The reason behind this asymmetry in field and optical chirality between Figs. 6(a) and 6(c) is the coupling of the incident wave to a different system mode in the two cases, as observed and discussed also in Ref. [35]. This asymmetry can have significant impact in sensing schemes like the one discussed here (i.e., layer under sensing between loss and gain slabs), indicating a wrong and a right incidence side for enhanced sensing signals. In addition to the above-mentioned asymmetry, one can observe also from Figs. 6(a) and 6(c) that the fields and optical chirality are symmetric in the gain and loss slabs, as expected for *PT*-symmetric systems at ATR points [35]. (Note that the presence of the chiral layer breaks the exact *PT* symmetry of the gain-loss bilayer; due to its very small thickness, the chiral layer acts as a small perturbation, allowing the system to preserve the basic characteristics of the exact *PT* case.)

In Figs. 6(b) and 6(d), we show the same results as in (a) and (c) at a CD peak of the same system [at frequency 623.9 THz, where the highest CD peak is observed—see Fig. 2(b)]. Here, as expected, we observe very strong field and optical chirality enhancement inside the system and particularly at its center, i.e., at the location of the chiral layer, while again here, the incidence from the gain side leads to higher field and optical chirality values than the incidence from the loss
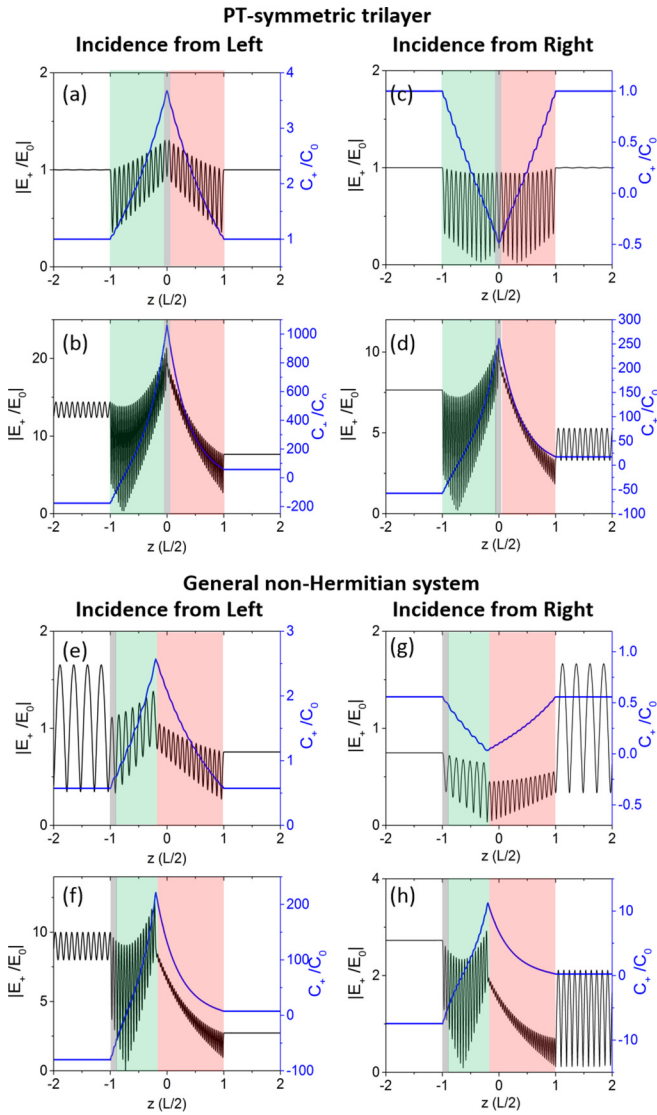
FIG. 6. Normalized electric fields and optical chirality calculations for the two systems of Figs. 2(b) and 2(c), for right-handed circularly polarized (RCP) waves incident from the left side (left column) and from the right side (right column). (a)–(d) correspond to the *PT*-symmetric system [of Fig. 2(b)], and (e)–(h) correspond to the general non-Hermitian system [of Fig. 2(c)]. (a), (c), (e), and (g) concern frequencies of dissymmetry factor peaks and (b), (d), (f), and (h) frequencies of circular dichroism (CD) peaks. The material parameters are the same as in Fig. 2, and we assume positive sign of the chirality parameter of the thin chiral layer (both real and imaginary parts). L is the total system length.

side. Moreover, the fields and optical chirality are not symmetric anymore between gain and loss layers, showing that this frequency is beyond the exceptional point of the system, as expected for *PT*-symmetric systems at the lasing threshold point and as verified from related scattering matrix calculations (see Appendix D).

In Figs. 6(e)–6(h), we plot the normalized electric field amplitude and the optical chirality along the system for the general non-Hermitian system of Fig. 2(c) (for RCP wave propagation). Specifically, Figs. 6(e) and 6(g) concern *g*-peak
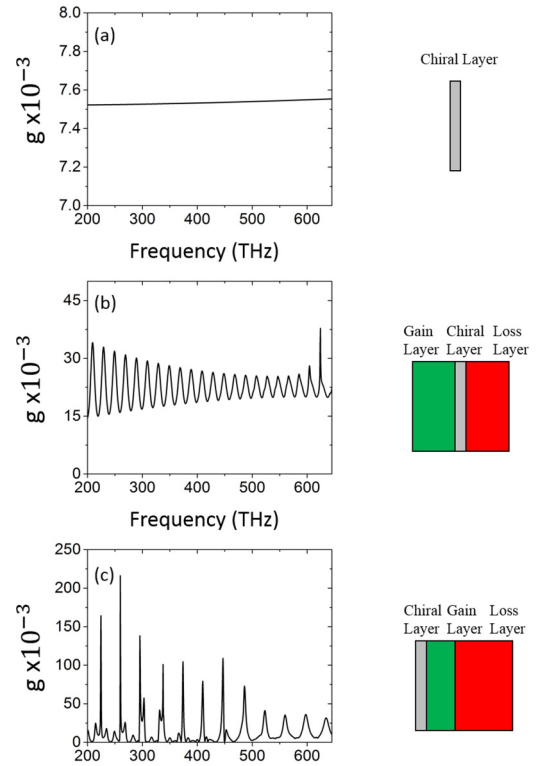

FIG. 7. Kuhn's dissymmetry factor (*g*) calculated considering the absorption only inside the chiral layer for the systems of Fig. 2. In all cases, we assume positive sign of the chirality parameter (both real and imaginary parts) of the thin chiral layer.

frequencies {246.6 THz for waves incident from the left side [Fig. 6(e)] and 246.85 THz for waves incident from the right side [Fig. 6(g)]} and Figs. 6(f) and 6(h) a CD-resonance frequency [617 THz—see Fig. 2(c)].

Observing the results of Fig. 6, one can see that, at the *g*-peak frequencies, the field intensity and the optical chirality (for both the *PT* and the non-*PT* trilayer) in the region of the chiral layer are considerably higher than their incident/vacuum values, ensuring increase of both differential and overall absorption, critical for enhanced chiro-optical response.

To investigate further the impact of the gain-loss bilayer on the chiro-optical response of our chiral layer, we calculate the local dissymmetry factor in our systems under investigation, i.e., the dissymmetry factor evaluated by considering the absorption only inside the chiral layer. For that, we employ the formula of Eq. (1), right-hand side (derived in Appendix F), integrating both numerator and denominator over the extent of the thin chiral layer only—see Eqs. (F10) and (F13). For simplicity, we assume only the positive values for the chirality parameter of the chiral layer; we also consider incidence from the left (gain) side, which appeared to be the proper side, i.e., the side maximizing the fields, according to the previous discussion (in connection with Fig. 6). For comparison, we calculate first the dissymmetry factor for the chiral layer alone—see Fig. 7(a). (The results, as expected, are the same as the corresponding ones of Fig. 4.) Then we repeat the calculations considering the presence of the gain and loss

layers (both for the *PT*-symmetric case and for the general non-Hermitian case).

In the case of the *PT*-symmetric trilayer, we observe that, at a broad frequency range, local *g* shows an up to fivefold increase due to the presence of the gain-loss bilayer, while it remains always $>2\times$ the single chiral layer value. In the case of the general non-Hermitian structure [Fig. 7(c)], the enhancement is more irregular, but it achieves even higher values. Note that the *g* enhancement shown in Figs. 4 and 7 is achieved without imposing any nanostructuring in the systems, which would lead to even more enhanced local fields and possibly enhanced local field chirality. Combining our approach (i.e., the gain approach) with such a nanostructuring (as, e.g., in Refs. [9,10]), we expect an additive effect, leading to particularly high *g* factors and opening prospects in the chirality detection and synthesis.

As a closing remark, we want to mention that the purpose of this paper is mostly to illustrate the potential and perspective of the combined gain-loss systems for CD and *g* enhancement, rather than to provide detailed guidelines for design of realistic systems. That is why we employ systems of constant gain and loss values within the whole optical range. For the realization of practical gain-loss systems for chirality detection enhancement, one can use a variety of active media, depending on the desired operation frequency. Critical requirements are (a) the spectral overlapping of the gain material bandwidth with resonances of the structure; (b) a spatial (modal) coupling of gain, loss, and chiral materials via close proximity; and (c) the chiral material being placed in contact with the gain material and, if possible, illuminated by the gain side. To satisfy the above requirements ensuring also maximum structure performance (e.g., operation close to the lasing threshold for maximum CD enhancement) is not straightforward, requiring also guiding by detailed numerical simulations. As our results suggest, even if the maximum performance regarding the CD is not achieved, there will always be substantial dissymmetry factor enhancement, as such an enhancement does not require operation close to the lasing threshold and can be encountered in a broad frequency range.

Regarding the gain materials that can be employed for the realization of suitable gain-loss systems, possible candidates can be dye molecules (they demonstrate a gain parameter of $\gamma = 4\pi \, \mathrm{Im}[n]/\lambda = 1590 \, \mathrm{cm}^{-1}$ at wavelength $\lambda = 710$ nm [61] and the half-width of the resonance 6000 nm), quantum wells or dots (with gain parameter of $\gamma = 5000 \, \mathrm{cm}^{-1}$ at wavelength $\lambda = 710$ nm [62]), two-dimensional transition metal dichalcogenides (with gain parameter up to $\gamma = 3 \times 10^4 \, \mathrm{cm}^{-1}$ at wavelength $\lambda = 640$ nm [63]), and others [59,64].

VII. CONCLUSIONS

We investigated non-Hermitian (i.e., combined gain-loss) systems, both *PT* symmetric and non-*PT* symmetric, for enhancement of chiro-optical signals of a thin chiral layer incorporated in those systems. By both analytical calculations and numerical modeling, we found that, in the *PT*-symmetric case, the CD and the dissymmetry factor *g* of the thin chiral layer placed between the gain and loss media can be enhanced by $75\times$ and $7\times$, respectively, compared with the chiral layer alone. The largest CD enhancement was obtained at the lasing

threshold of the total system and the largest *g* factor at its ATRs; a particularly interesting and useful feature is that the *g*-factor enhancement here is also associated with total field enhancement. Departing from the exact *PT*-symmetry condition for the gain and loss layers and going to systems more amenable to practical realization, we still found considerable CD and *g* enhancement, in some cases, even more intense than in the *PT* case. Although our approach concerns a resonant, essentially double-layer, gain-loss structure, it clearly reveals the rich possibilities offered by going to more complex structures, e.g., multistack *PT*-symmetric structures [35,49]; adding more layers, we may be able to create an even more enhanced response, enhancing the field and its confinement around the chiral layer.

Our results clearly demonstrate the potential of gain materials and of combined gain-loss media for chirality sensing. Moreover, our approach can be applied in combination with other optical approaches that have been proposed for chiro-optical signal enhancement, expanding the potential of those approaches and leading to photonic schemes for chiral biosensing.

Although this paper concerns a simple route for chirality enhancement in a thin chiral layer, it clearly reveals the rich possibilities offered by combining gain and loss. We expect those possibilities to be even more enhanced and exploitable in other weak electromagnetic phenomena, particularly associated with nonreciprocal materials, e.g., magneto-optical materials [65,66], where the combination of gain and loss with the system resonances may lead to even larger enhancements, opening directions in the field of non-Hermitian photonics.

APPENDIX A: ANALYTICAL CALCULATION OF THE REFLECTION AND TRANSMISSION FOR THE THREE-LAYER SYSTEM—THE CHIRAL TRANSFER MATRIX METHOD

To find the reflection and transmission amplitudes of the three-layer (gain, chiral, and loss) structure shown in Fig. 1 of the main text, we consider waves arriving at normal incidence from either side of the structure, and we solve Maxwell's equations, applying the boundary conditions at each interface. The waves propagate along the *z* direction, as illustrated in Fig. 1, and their polarization can be either linear or circular. We start with layers with arbitrary material parameters ε_i, μ_i, and κ_i to obtain general expressions (the subscript $i = \{G, C, L\}$ denotes the gain, chiral, and loss regions, respectively). Due to the two possible input circular polarizations (denoted as RCP/+ and LCP/−) at each of the two sides of the system, the full description of the scattering process requires four input and four output ports; hence, the system

is described by a 4×4 scattering matrix, consisting of eight transmission (t) and eight reflection (r) coefficients.

To determine the reflection and transmission coefficients, we assume that we have either RCP/+ or LCP/− polarized incident plane waves, arriving from the left side (see Fig 1):

$$
\begin{aligned}
\mathbf{E}_{\text{in}}^{\text{air}} &= a_\pm \hat{\mathbf{e}}_\pm e^{ikz}, \\
\mathbf{H}_{\text{in}}^{\text{air}} &= \mp i Z^{-1} a_\pm \hat{\mathbf{e}}_\pm e^{ikz},
\end{aligned}
\tag{A1}
$$

(the structure is embedded in air, and the subscript "in" denotes the incident wave). The reflected electromagnetic fields can be expressed as

$$
\begin{aligned}
\mathbf{E}_{\text{ref}}^{\text{air}} &= -b_+ \hat{\mathbf{e}}_- e^{-ikz} - b_- \hat{\mathbf{e}}_+ e^{-ikz}, \\
\mathbf{H}_{\text{ref}}^{\text{air}} &= -i Z^{-1}(-b_+)\hat{\mathbf{e}}_- e^{-ikz} + i Z^{-1}(-b_-)\hat{\mathbf{e}}_+ e^{-ikz},
\end{aligned}
\tag{A2}
$$

where $a_\pm$ and $b_\pm$ are the amplitudes of the ingoing and outgoing, respectively, RCP/+ and LCP/− waves (as observed from the source point), and $\hat{\mathbf{e}}_\pm = (\hat{\mathbf{x}} \pm i\hat{\mathbf{y}})/\sqrt{2}$. A similar expression can be employed for electric and magnetic fields inside the gain, loss, and chiral layers, where the total field is a sum of a forward- and a backward-propagating wave. In the chiral layer, due to the two different refractive indices $n_\pm = \sqrt{\mu\varepsilon} \pm \kappa$, we have different wave vectors for the RCP and LCP components. Thus, in the chiral layer, the electromagnetic field can be expressed as

$$
\begin{aligned}
\mathbf{E}_{\text{forw}}^{\text{chiral}} &= E_+^{(\text{L})}\hat{\mathbf{e}}_+ e^{ik_+z} + E_- \hat{\mathbf{e}}_- e^{ik_-z}, \\
\mathbf{H}_{\text{forw}}^{\text{chiral}} &= \mp i Z^{-1}\big[E_+^{(\text{L})}\hat{\mathbf{e}}_+ e^{ik_+z} + E_- \hat{\mathbf{e}}_- e^{ik_-z}\big],
\end{aligned}
\tag{A3}
$$

and

$$
\begin{aligned}
\mathbf{E}_{\text{back}}^{\text{chiral}} &= -E_+^{(\text{R})}\hat{\mathbf{e}}_- e^{-ik_-z} - E_- \hat{\mathbf{e}}_+ e^{-ik_+z}, \\
\mathbf{H}_{\text{back}}^{\text{chiral}} &= \mp i Z^{-1}\big[-E_+^{(\text{R})}\hat{\mathbf{e}}_- e^{-ik_-z} - E_- \hat{\mathbf{e}}_+ e^{-ik_+z}\big].
\end{aligned}
\tag{A4}
$$

The transmitted electromagnetic fields can be expressed as

$$
\begin{aligned}
\mathbf{E}_{\text{tr}}^{\text{air}} &= c_+ \hat{\mathbf{e}}_+ e^{ikz} + c_- \hat{\mathbf{e}}_- e^{ikz}, \\
\mathbf{H}_{\text{tr}}^{\text{air}} &= -i Z^{-1} c_+ \hat{\mathbf{e}}_+ e^{ikz} + i Z^{-1} c_- \hat{\mathbf{e}}_- e^{ikz},
\end{aligned}
\tag{A5}
$$

where $c_\pm$ are the amplitudes of the transmitted waves (see Fig. 1). Equating the tangential components of $\mathbf{E}$ and $\mathbf{H}$ (E_x, E_y, H_x, H_y) at the four structure interfaces, we obtain a 16×16 linear system of equations with 72 out of 256 nonzero elements, which is solved analytically or numerically (using, for example, Gaussian elimination with the partial pivot method),

giving the scattering coefficients (for more detailed analysis regarding the methodology, see Refs. [10,51]). The reflection and transmission coefficients when the incident wave arrives from the right side of the structure can be obtained by applying the same analysis as above or, more easily, by exchanging the material parameters in the gain-loss layers.

Although, in this paper, we focus on the analytical derivation (although cumbersome yet straightforward) of the reflection and transmission coefficients for a three-layer system, we consider it useful to provide a derivation approach that can be extended to multilayer systems, being also more compact in the formalism. Such an approach is provided by the transfer matrix method. Therefore, we present below the transfer matrix formalism in circular polarization basis, suitable for the analysis of electromagnetic wave propagation in multilayer structures (including chiral layers), under normal incidence. The transfer matrix M relates the fields on one side of an interface to those of the other side (see Fig. 1 for the definition of field amplitudes). Because the electric field in the circular polarization basis is described by four waves, two (LCP/+ and RCP/− as a source view) incident on the interface and the other two outgoing, the matching matrix M is a 4×4 matrix of the form:

$$
\begin{pmatrix} a_+ \\ a_- \\ b_+ \\ b_- \end{pmatrix}_i = M_{i,i+1} \begin{pmatrix} c_+ \\ c_- \\ d_+ \\ d_- \end{pmatrix}_{i+1},
\tag{A6}
$$

where i (counting the layers) denotes the layer left to the interface, and $M_{i,i+1}$ is block symmetric of the form $M_{i,i+1} = \begin{pmatrix} A & B \\ B & A \end{pmatrix}$, with the corresponding submatrices given by

$$
A = \begin{pmatrix} \frac{1}{2}\big(\frac{Z_i}{Z_{i+1}} + 1\big) & 0 \\ 0 & \frac{1}{2}\big(\frac{Z_i}{Z_{i+1}} + 1\big) \end{pmatrix},
\tag{A7}
$$

$$
B = \begin{pmatrix} 0 & \frac{1}{2}\big(\frac{Z_i}{Z_{i+1}} - 1\big) \\ \frac{1}{2}\big(\frac{Z_i}{Z_{i+1}} - 1\big) & 0 \end{pmatrix}.
\tag{A8}
$$

Referring to Fig. 1, the fields on the left side of the system and those on the right side are connected with the total transfer matrix $M^{(\text{total})}$. For the construction of $M^{(\text{total})}$, in addition to the transfer matrices of the individual interfaces, one must also consider the phase matrices. A phase matrix P_i accounts for the phase contributed by forward and backward waves propagating inside the medium i, with a thickness of d_i, and is given by

$$
P_i = \begin{pmatrix}
\exp[ik_+^{(i)}d_i] & 0 & 0 & 0 \\
0 & \exp[ik_-^{(i)}d_i] & 0 & 0 \\
0 & 0 & \exp[-ik_+^{(i)}d_i] & 0 \\
0 & 0 & 0 & \exp[-ik_-^{(i)}d_i]
\end{pmatrix}.
\tag{A9}
$$

For nonchiral layers, the P_i matrices can be simplified by taking $k_+^{(i)} = k_-^{(i)} = k^{(i)}$. The system of multilayers can then be solved by the ordered multiplication of interface transfer matrices $M_{i,i+1}$ and the in-layer phase matrices P_i. The resulting transfer matrix $M^{(\text{total})}$ contains all the wave reflection and transmission information for the system. For the

gain-chiral-loss system of Fig. 1, the total transfer matrix is given by

$$
\begin{pmatrix} a_+ \\ a_- \\ b_+ \\ b_- \end{pmatrix} = M^{(\text{total})} \begin{pmatrix} c_+ \\ c_- \\ d_+ \\ d_- \end{pmatrix} \equiv M_{01} P_1 M_{12} P_2 M_{23} P_3 M_{34} \begin{pmatrix} c_+ \\ c_- \\ d_+ \\ d_- \end{pmatrix},
\tag{A10}
$$

where the subscripts 0 and 4 correspond to the layers before and after the structure, respectively (both air in our case). Having evaluated the transfer matrix $M^{(\text{total})}$, one can decompose it in four 2×2 submatrices, of the form $M^{(\text{total})} = \begin{pmatrix} T_1 & R_1 \\ R_2 & T_2 \end{pmatrix}$. Then the reflection and transmission matrices for incidence from the left side of the system are given by $R^{(\text{L})} = \begin{pmatrix} r_{++}^{(\text{L})} & r_{+-}^{(\text{L})} \\ r_{-+}^{(\text{L})} & r_{--}^{(\text{L})} \end{pmatrix} = R_2 (T_1)^{-1}$ and $T^{(\text{L})} = \begin{pmatrix} t_{++}^{(\text{L})} & t_{+-}^{(\text{L})} \\ t_{-+}^{(\text{L})} & t_{--}^{(\text{L})} \end{pmatrix} = (T_1)^{-1}$ and for incidence from the right side are given by $R^{(\text{R})} = \begin{pmatrix} r_{++}^{(\text{R})} & r_{+-}^{(\text{R})} \\ r_{-+}^{(\text{R})} & r_{--}^{(\text{R})} \end{pmatrix} = -(T_1)^{-1} R_1$ and $T^{(\text{R})} = \begin{pmatrix} t_{++}^{(\text{R})} & t_{+-}^{(\text{R})} \\ t_{-+}^{(\text{R})} & t_{--}^{(\text{R})} \end{pmatrix} = T_2 - R_2 (T_1)^{-1} R_1$ [67,68].

For layers of isotropic chiral materials (reciprocal) and normal incidence, it is in general valid, that $t_{++}^{(\text{L})} = t_{++}^{(\text{R})}$, $t_{--}^{(\text{L})} = t_{--}^{(\text{R})}$ and $r_{+-}^{(\text{L})} = r_{-+}^{(\text{L})}$, $r_{+-}^{(\text{R})} = r_{-+}^{(\text{R})}$, while the remaining eight coefficients $r_{++}^{(\text{L})} = r_{--}^{(\text{L})} = r_{++}^{(\text{R})} = r_{--}^{(\text{R})} = t_{+-}^{(\text{L})} = t_{-+}^{(\text{L})} = t_{+-}^{(\text{R})} = t_{-+}^{(\text{R})} = 0$ regardless of the side of incidence. The analytical expressions of r and t for circularly and linearly polarized waves are listed below.

Scattering coefficients for CP waves
Incident from left:

$$
t_{++}^{(\text{L})} = -\frac{16 \exp\{i[d_C(k - k_\text{G} - k_\text{L}) + d(2k - k_\text{G} - k_\text{L})]\}}{Z_\text{G} Z_\text{C} Z_\text{L}(A_1 + A_2 + B_1 + B_2)} \exp(ik_{C1}d_C),
$$

$$
t_{--}^{(\text{L})} = -\frac{16 \exp\{i[d_C(k - k_\text{G} - \text{k}_\text{L}) + d(2k - k_\text{G} - k_\text{L})]\}}{Z_\text{G} Z_\text{C} Z_\text{L}(A_1 + A_2 + B_1 + B_2)} \exp(ik_{C2}d_C),
$$

$$
t_{-+}^{(\text{L})} = t_{+-}^{(\text{L})} = 0,
$$

$$
r_{+-}^{(\text{L})} = r_{-+}^{(\text{L})} = \frac{\exp\left[-2ik\left(d + \frac{d_c}{2}\right)\right]\left[C_1^{(\text{L})} + C_2^{(\text{L})} + D_1^{(\text{L})} + D_2^{(\text{L})}\right]}{(A_1 + A_2 + B_1 + B_2)},
$$

$$
r_{++}^{(\text{L})} = r_{--}^{(\text{L})} = 0.
\tag{A11}
$$

Incident from right:

$$
t_{++}^{(\text{R})} = -\frac{16 \exp\{i[d_C(k - k_\text{G} - k_\text{L}) + d(2k - k_\text{G} - k_\text{L})]\}}{Z_\text{G} Z_\text{C} Z_\text{L}(A_1 + A_2 + B_1 + B_2)} \exp(ik_{C1}d_C),
$$

$$
t_{--}^{(\text{R})} = -\frac{16 \exp\{i[d_C(k - k_\text{G} - k_\text{L}) + d(2k - k_\text{G} - k_\text{L})]\}}{Z_\text{G} Z_\text{C} Z_\text{L}(A_1 + A_2 + B_1 + B_2)} \exp(ik_{C2}d_C),
$$

$$
t_{-+}^{(\text{R})} = t_{+-}^{(\text{R})} = 0,
$$

$$
r_{+-}^{(\text{R})} = r_{-+}^{(\text{R})} = \frac{\exp\left[-2ik(d + \frac{d_c}{2})\right]\left[C_1^{(\text{R})} + C_2^{(\text{R})} + D_1^{(\text{R})} + D_2^{(\text{R})}\right]}{(A_1 + A_2 + B_1 + B_2)},
$$

$$
r_{++}^{(\text{R})} = r_{--}^{(\text{R})} = 0.
\tag{A12}
$$

Scattering coefficients for linearly polarized waves
Incident from left, x polarized:

$$
t_{xx}^{(\text{L})} = -\frac{8 \exp\{-i[d_C(k - k_\text{G} - k_\text{L}) + d(2k - k_\text{G} - k_\text{L})]\}}{Z_\text{G} Z_\text{C} Z_\text{L}(A_1 + A_2 + B_1 + B_2)} [\exp(ik_{C1}d_C) + \exp(ik_{C2}d_C)],
$$

$$
t_{yx}^{(\text{L})} = -i\frac{8 \exp\{-i[d_C(k - k_\text{G} - k_\text{L}) + d(2k - k_\text{G} - k_\text{L})]\}}{Z_\text{G} Z_\text{C} Z_\text{L}(A_1 + A_2 + B_1 + B_2)} [\exp(ik_{C1}d_C) - \exp(ik_{C2}d_C)],
$$

$$
r_{xx}^{(\text{L})} = \frac{\exp\left[-2ik\left(d + \frac{d_c}{2}\right)\right]\left[C_1^{(\text{L})} + C_2^{(\text{L})} + D_1^{(\text{L})} + D_2^{(\text{L})}\right]}{(A_1 + A_2 + B_1 + B_2)},
$$

$$
r_{yx}^{(\text{L})} = 0.
\tag{A13}
$$

Incident from right, x polarized:

$$t_{xx}^{(R)} = t_{xx}^{(L)},$$
$$t_{yx}^{(R)} = -t_{yx}^{(L)},$$
$$r_{xx}^{(R)} = \frac{\exp\left[-2ik\left(d + \frac{d_c}{2}\right)\right]\left[C_1^{(R)} + C_2^{(R)} + D_1^{(R)} + D_2^{(R)}\right]}{(A_1 + A_2 + B_1 + B_2)},$$
$$r_{yx}^{(R)} = 0. \tag{A14}$$

Incident from left, y polarized:

$$t_{yy}^{(L)} = t_{xx}^{(L)},$$
$$t_{xy}^{(L)} = -t_{yx}^{(L)},$$
$$r_{yy}^{(L)} = r_{xx}^{(L)},$$
$$r_{xy}^{(L)} = r_{yx}^{(L)}. \tag{A15}$$

Incident from right, y polarized:

$$t_{yy}^{(R)} = t_{xx}^{(R)},$$
$$t_{xy}^{(R)} = -t_{yx}^{(R)},$$
$$r_{yy}^{(R)} = r_{xx}^{(R)},$$
$$r_{xy}^{(R)} = r_{yx}^{(R)}. \tag{A16}$$

In the above formulas Eqs. (A11)–(A16), the superscripts (L) and (R) denote incidence from the left and right side of the system, respectively, the first subscript in r and t denotes the output polarization and the second the input polarization, and

$$
\begin{aligned}
A_1 &= \exp\left[2i\left(d + \frac{d_C}{2}\right)(k_G + k_L)\right]\left(\frac{1}{Z_G} - 1\right)\left(\frac{1}{Z_G} - \frac{1}{Z_C}\right)\left(\frac{1}{Z_C} - \frac{1}{Z_L}\right)\left(\frac{1}{Z_L} - 1\right) \\
&\quad - \exp\left\{2i\left[k_L d + \frac{(k_G + k_L)d_C}{2}\right]\right\}\left(\frac{1}{Z_G} + 1\right)\left(\frac{1}{Z_G} + \frac{1}{Z_C}\right)\left(\frac{1}{Z_C} - \frac{1}{Z_L}\right)\left(\frac{1}{Z_L} - 1\right), \\
A_2 &= -\exp[id_C(k_G + k_{C1} + k_{C2} + k_L)]\left(\frac{1}{Z_G} + 1\right)\left(\frac{1}{Z_G} - \frac{1}{Z_C}\right)\left(\frac{1}{Z_C} - \frac{1}{Z_L}\right)\left(\frac{1}{Z_L} + 1\right) \\
&\quad + \exp\left\{2i\left[k_G d + \frac{(k_G + k_{C1} + k_{C2} + k_L)d_C}{2}\right]\right\}\left(\frac{1}{Z_G} - 1\right)\left(\frac{1}{Z_G} + \frac{1}{Z_C}\right)\left(\frac{1}{Z_C} - \frac{1}{Z_L}\right)\left(\frac{1}{Z_L} + 1\right), \\
B_1 &= -\exp\left\{2i\left[k_L d + \frac{(k_G + k_{C1} + k_{C2} + k_L)d_C}{2}\right]\right\}\left(\frac{1}{Z_G} + 1\right)\left(\frac{1}{Z_G} - \frac{1}{Z_C}\right)\left(\frac{1}{Z_C} + \frac{1}{Z_L}\right)\left(\frac{1}{Z_L} - 1\right) \\
&\quad + \exp\left\{2i\left[(k_G + k_L)d + \frac{(k_G + k_{C1} + k_{C2} + k_L)d_C}{2}\right]\right\}\left(\frac{1}{Z_G} - 1\right)\left(\frac{1}{Z_G} + \frac{1}{Z_C}\right)\left(\frac{1}{Z_C} + \frac{1}{Z_L}\right)\left(\frac{1}{Z_L} - 1\right), \\
B_2 &= \exp\left\{2i\left[k_G d + \frac{(k_G + k_L)d_C}{2}\right]\right\}\left(\frac{1}{Z_G} - 1\right)\left(\frac{1}{Z_G} - \frac{1}{Z_C}\right)\left(\frac{1}{Z_C} + \frac{1}{Z_L}\right)\left(\frac{1}{Z_L} + 1\right) \\
&\quad - \exp[i(k_G + k_L)d_C]\left(\frac{1}{Z_G} + 1\right)\left(\frac{1}{Z_G} + \frac{1}{Z_C}\right)\left(\frac{1}{Z_C} + \frac{1}{Z_L}\right)\left(\frac{1}{Z_L} + 1\right). \tag{A17} \\
C_1^{(L)} &= -\exp\left[2i\left(d + \frac{d_C}{2}\right)(k_G + k_L)\right]\left(\frac{1}{Z_G} + 1\right)\left(\frac{1}{Z_G} - \frac{1}{Z_C}\right)\left(\frac{1}{Z_C} - \frac{1}{Z_L}\right)\left(\frac{1}{Z_L} - 1\right) \\
&\quad + \exp\{2i[k_L d + (k_G + k_L)d_C/2]\}\left(\frac{1}{Z_G} - 1\right)\left(\frac{1}{Z_G} + \frac{1}{Z_C}\right)\left(\frac{1}{Z_C} - \frac{1}{Z_L}\right)\left(\frac{1}{Z_L} - 1\right), \\
C_2^{(L)} &= \exp[id_C(k_G + k_{C1} + k_{C2} + k_L)]\left(\frac{1}{Z_G} - 1\right)\left(\frac{1}{Z_G} - \frac{1}{Z_C}\right)\left(\frac{1}{Z_C} - \frac{1}{Z_L}\right)\left(\frac{1}{Z_L} + 1\right) \\
&\quad - \exp\left\{2i\left[k_G d + \frac{(k_G + k_{C1} + k_{C2} + k_L)d_C}{2}\right]\right\}\left(\frac{1}{Z_G} + 1\right)\left(\frac{1}{Z_G} + \frac{1}{Z_C}\right)\left(\frac{1}{Z_C} - \frac{1}{Z_L}\right)\left(\frac{1}{Z_L} + 1\right),
\end{aligned}
$$

$$D_1^{(L)} = \exp\left\{2i\left[k_L d + \frac{(k_G + k_{C1} + k_{C2} + k_L)d_C}{2}\right]\right\}\left(\frac{1}{Z_G} - 1\right)\left(\frac{1}{Z_G} - \frac{1}{Z_C}\right)\left(\frac{1}{Z_C} + \frac{1}{Z_L}\right)\left(\frac{1}{Z_L} - 1\right)$$

$$- \exp\left\{2i\left[(k_G + k_L)d + \frac{(k_G + k_{C1} + k_{C2} + k_L)d_C}{2}\right]\right\}\left(\frac{1}{Z_G} + 1\right)\left(\frac{1}{Z_G} + \frac{1}{Z_C}\right)\left(\frac{1}{Z_C} + \frac{1}{Z_L}\right)\left(\frac{1}{Z_L} - 1\right),$$

$$D_2^{(L)} = -\exp\left\{2i\left[k_G d + \frac{(k_G + k_L)d_C}{2}\right]\right\}\left(\frac{1}{Z_G} + 1\right)\left(\frac{1}{Z_G} - \frac{1}{Z_C}\right)\left(\frac{1}{Z_C} + \frac{1}{Z_L}\right)\left(\frac{1}{Z_L} + 1\right)$$

$$+ \exp[i(k_G + k_L)d_C]\left(\frac{1}{Z_G} - 1\right)\left(\frac{1}{Z_G} + \frac{1}{Z_C}\right)\left(\frac{1}{Z_C} + \frac{1}{Z_L}\right)\left(\frac{1}{Z_L} + 1\right). \tag{A18}$$

$$C_1^{(R)} = -\exp\left[2i\left(d + \frac{d_C}{2}\right)(k_G + k_L)\right]\left(\frac{1}{Z_L} + 1\right)\left(\frac{1}{Z_L} - \frac{1}{Z_C}\right)\left(\frac{1}{Z_C} - \frac{1}{Z_G}\right)\left(\frac{1}{Z_G} - 1\right)$$

$$+ \exp\{2i[k_G d + (k_G + k_L)d_C/2]\}\left(\frac{1}{Z_L} - 1\right)\left(\frac{1}{Z_L} + \frac{1}{Z_C}\right)\left(\frac{1}{Z_C} - \frac{1}{Z_G}\right)\left(\frac{1}{Z_G} - 1\right),$$

$$C_2^{(R)} = \exp[id_C(k_G + k_{C1} + k_{C2} + k_L)]\left(\frac{1}{Z_L} - 1\right)\left(\frac{1}{Z_L} - \frac{1}{Z_C}\right)\left(\frac{1}{Z_C} - \frac{1}{Z_G}\right)\left(\frac{1}{Z_G} + 1\right)$$

$$- \exp\left\{2i\left[k_L d + \frac{(k_G + k_{C1} + k_{C2} + k_L)d_C}{2}\right]\right\}\left(\frac{1}{Z_G} + 1\right)\left(\frac{1}{Z_G} + \frac{1}{Z_C}\right)\left(\frac{1}{Z_C} - \frac{1}{Z_L}\right)\left(\frac{1}{Z_L} + 1\right),$$

$$D_1^{(R)} = \exp\left\{2i\left[k_G d + \frac{(k_G + k_{C1} + k_{C2} + k_L)d_C}{2}\right]\right\}\left(\frac{1}{Z_L} - 1\right)\left(\frac{1}{Z_L} - \frac{1}{Z_C}\right)\left(\frac{1}{Z_C} + \frac{1}{Z_G}\right)\left(\frac{1}{Z_G} - 1\right)$$

$$- \exp\left\{2i\left[(k_G + k_L)d + \frac{(k_G + k_{C1} + k_{C2} + k_L)d_C}{2}\right]\right\}\left(\frac{1}{Z_L} + 1\right)\left(\frac{1}{Z_L} + \frac{1}{Z_C}\right)\left(\frac{1}{Z_C} + \frac{1}{Z_G}\right)\left(\frac{1}{Z_G} - 1\right),$$

$$D_2^{(R)} = -\exp\left\{2i\left[k_L d + \frac{(k_G + k_L)d_C}{2}\right]\right\}\left(\frac{1}{Z_L} + 1\right)\left(\frac{1}{Z_L} - \frac{1}{Z_C}\right)\left(\frac{1}{Z_C} + \frac{1}{Z_G}\right)\left(\frac{1}{Z_G} + 1\right)$$

$$+ \exp[i(k_G + k_L)d_C]\left(\frac{1}{Z_L} - 1\right)\left(\frac{1}{Z_L} + \frac{1}{Z_C}\right)\left(\frac{1}{Z_C} + \frac{1}{Z_G}\right)\left(\frac{1}{Z_G} + 1\right). \tag{A19}$$

In the above relations, $Z_i = \sqrt{\mu_0\mu_i/\varepsilon_0\varepsilon_i}$, $i = \{G, C, L\}$, is the wave impedance, and $k_G = \frac{\omega(\sqrt{\varepsilon_G\mu_G})}{c}$, $k_L = \frac{\omega(\sqrt{\varepsilon_L\mu_L})}{c}$, and $k_{C1} = \frac{\omega(\sqrt{\varepsilon_C\mu_C}+\kappa)}{c}$, $k_{C2} = \frac{\omega(\sqrt{\varepsilon_C\mu_C}-\kappa)}{c}$ are the wave vectors in the gain, loss, and chiral regions, respectively.

APPENDIX B: DERIVATION OF EQS. (2)–(4)

In this section, we calculate the CD and the dissymmetry factor g for the system shown in Fig. 1 of the main text with *PT*-symmetric gain-loss layers. To calculate the CD and g, it is necessary to calculate the absorption amplitudes for RCP and LCP waves. According to the scattering matrix S theory [67], the main diagonal of the difference $\hat{1} - S^\dagger S$ (where $\hat{1}$ is the identity matrix and † means a transpose and complex conjugate) contains the absorption amplitudes for different circular polarizations (RCP/+)-(LCP/−) and sides of incidence. We express them as

$$A_+^{(L)} = 1 - |r_{-+}^{(L)}|^2 - |t_{++}^{(L)}|^2,$$

$$A_-^{(R)} = 1 - |r_{+-}^{(R)}|^2 - |t_{--}^{(R)}|^2,$$

$$A_-^{(L)} = 1 - |r_{+-}^{(L)}|^2 - |t_{--}^{(L)}|^2,$$

$$A_+^{(R)} = 1 - |r_{-+}^{(R)}|^2 - |t_{++}^{(R)}|^2. \tag{B1}$$

In the previous section, we found that $t_{++}^{(L)} = t_{++}^{(R)} \equiv t_{++}$ and $t_{--}^{(L)} = t_{--}^{(R)} \equiv t_{--}$ (reciprocal system), while $r_{-+}^{(L)} = r_{+-}^{(L)} \equiv r^{(L)}$ and $r_{+-}^{(R)} = r_{-+}^{(R)} \equiv r^{(R)}$; therefore, CD = $A_+ - A_-$ becomes

$$CD^{(L)} = CD^{(R)} \equiv CD = |t_{--}|^2 - |t_{++}|^2. \tag{B2}$$

Inserting the transmission coefficients from Eq. (A11) into Eq. (B2), we find

$$CD = \frac{256\exp(-2\{\text{Im}(k_{C1}d_C) + \text{Im}(k_{C2}d_C) + \text{Im}[d_C(k - k_G - k_L) + d(2k - k_G - k_L)]\})}{|Z_G Z_C Z_L (A_1 + A_2 + B_1 + B_2)|^2}\{\exp[2\text{Im}(k_{C1}d_C)]e^{2\text{Im}(k_{C1}d_C)}$$

$$- \exp[2\text{Im}(k_{C2}d_C)]e^{2\text{Im}(k_{C2}d_C)}. \tag{B3}$$

In the case of PT-symmetric gain-loss layers, the wave vectors obey $k_G = (k_L)^*$; moreover $k_{C1} = \omega(n_C + \kappa)/c$, $k_{C2} = \omega(n_C - \kappa)/c$, where n_C and κ are the nonchiral refractive index and the chirality parameter of the chiral layer, respectively. After some algebra, the term $\exp[2\mathrm{Im}(k_{C1}d_C)] - \exp[2\mathrm{Im}(k_{C2}d_C)]$ in Eq. (B3) can be simplified as $2\exp(2kd_C\mathrm{Im}[n_C])\sinh(2kd_C\mathrm{Im}[\kappa])$ and the term $\exp(-2\{\mathrm{Im}(k_{C1}d_C) + \mathrm{Im}(k_{C2}d_C) + \mathrm{Im}[d_C(k - k_G - k_L) + d(2k - k_G - k_L)]\})$ can be expressed as $\exp(-4kd_C\mathrm{Im}[n_C])$. Hence, the CD in the PT case can be written [Eq. (2) of the main text] as

$$\mathrm{CD} = \frac{512\exp(-2kd_C\mathrm{Im}[n_C])}{|Z_G Z_C Z_L (A_1 + A_2 + B_1 + B_2)|^2} \sinh(2kd_C\mathrm{Im}[\kappa]), \tag{B4}$$

where the terms $A_1, A_2, B_1,$ and B_2 are given in the previous section and are totally independent of the chirality parameter κ.

For the calculation of the dissymmetry factor g defined as [7]

$$g = \frac{2\mathrm{CD}}{A_+ + A_-}, \tag{B5}$$

in addition to CD, one needs to also calculate the total absorption $A_+ + A_-$ (for RCP and LCP waves) for incidence from both system sides. From Eq. (B1), we see that the total absorption depends on the reflectance and therefore depends on the side of incidence, as

$$A_+^{(L)} + A_-^{(L)} = 1 - |r_{-+}^{(L)}|^2 - |t_{++}^{(L)}|^2 + 1 - |r_{+-}^{(L)}|^2 - |t_{--}^{(L)}|^2 \equiv 2 - |t_{++}|^2 - |t_{--}|^2 - 2|r^{(L)}|^2,$$

$$A_+^{(R)} + A_-^{(R)} = 1 - |r_{-+}^{(R)}|^2 - |t_{++}^{(R)}|^2 + 1 - |r_{+-}^{(R)}|^2 - |t_{--}^{(R)}|^2 \equiv 2 - |t_{++}|^2 - |t_{--}|^2 - 2|r^{(R)}|^2. \tag{B6}$$

By substituting Eqs. (B3) and (B6) into (B5) and after extensive but straightforward calculations, we obtain

$$g^{(L)} = -256\{\exp[2\mathrm{Im}(k_{C1}d_C)] - \exp[2\mathrm{Im}(k_{C2}d_C)]\}\left(\frac{1}{128\{\exp[2\mathrm{Im}(k_{C1}d_C)] + \exp[2\mathrm{Im}(k_{C2}d_C)]\}}\right.$$

$$- \frac{1}{P\exp\{2\mathrm{Im}[d_C(k - k_G + k_{C1} + k_{C2} - k_L) + d(2k - k_G - k_L)]\}}$$

$$\left.+ \frac{1}{Q^{(L)}\exp\{2\mathrm{Im}[d_C(k - k_G + k_{C1} + k_{C2} - k_L) + d(2k - k_G - k_L)]\}}\right) \tag{B7}$$

$$g^{(R)} = -256\{\exp[2\mathrm{Im}(k_{C1}d_C)] - \exp[2\mathrm{Im}(k_{C2}d_C)]\}\left(\frac{1}{128\{\exp[2\mathrm{Im}(k_{C1}d_C)] + \exp[2\mathrm{Im}(k_{C2}d_C)]\}}\right.$$

$$- \frac{1}{P\exp\{2\mathrm{Im}[d_C(k - k_G + k_{C1} + k_{C2} - k_L) + d(2k - k_G - k_L)]\}}$$

$$\left.+ \frac{1}{Q^{(R)}\exp\{2\mathrm{Im}[d_C(k - k_G + k_{C1} + k_{C2} - k_L) + d(2k - k_G - k_L)]\}}\right), \tag{B8}$$

where $P = |Z_G Z_C Z_L (A_1 + A_2 + B_1 + B_2)|^2$, $Q^{(L)} = |Z_G Z_C Z_L [C_1^{(L)} + C_2^{(L)} + D_1^{(L)} + D_2^{(L)}]|^2$, and $Q^{(R)} = |Z_G Z_C Z_L [C_1^{(R)} + C_2^{(R)} + D_1^{(R)} + D_2^{(R)}]|^2$. Considering the PT symmetry of the gain-loss layers, Eqs. (B7) and (B8) can be simplified as

$$g^{(L)} = -2\tanh(2kd_C\mathrm{Im}[\kappa]) + 512\exp(-2kd_C\mathrm{Im}[n_C])\sinh(2kd_C\mathrm{Im}[\kappa])\left[\frac{1}{P} + \frac{1}{Q^{(L)}}\right], \tag{B9}$$

$$g^{(R)} = -2\tanh(2kd_C\mathrm{Im}[\kappa]) + 512\exp(-2kd_C\mathrm{Im}[n_C])\sinh(2kd_C\mathrm{Im}[\kappa])\left[\frac{1}{P} + \frac{1}{Q^{(R)}}\right]. \tag{B10}$$

APPENDIX C: SCATTERING MATRIX APPROACH

It is often convenient to describe scattering systems in terms of their scattering matrix S. Among others, S can be used to identify and/or analyze exotic scattering phenomena such as PT-symmetric and broken-PT-symmetric phases, exceptional points, or ATRs [35,52,53]. The scattering matrix of a system describes the relation between its incoming and outgoing waves. In systems involving chiral media (and therefore interacting differently with RCP and LCP waves), such as the one of Fig. 1 of the main text, because of the two possible circular polarizations at each of the two sides of a system, it should be described by a 4×4 scattering matrix

S. Depending on the arrangement of the input and output ports (RCP or LCP waves), we can build the scattering matrix formalism in several ways. However, as the main information we want to extract is related to the position of the exceptional points (where a PT system passes from PT-symmetric phase to broken-PT phase) and of the ATRs, we will list here only the two relevant (as shown in the literature [35]) scattering matrix configurations along with their eigenvalues. The first configuration (case I), denoted here by $S^{(1)}$, is related to the position of exceptional point/points, i.e., the points at which $S^{(1)}$ eigenvalues stop being unimodular are exceptional points, where two or more eigenvalues and eigenvectors coincide.

In this definition, the reflection coefficients are on the diagonal, and the outgoing waves are related to the incident waves through time reversal. This behavior mimics the 2×2 matrix representation of *PT*-symmetric Hamiltonian [69] or *PT*-symmetric coupled optical waveguides [46] with the different reflected coefficients due to different wave impedances in the gain-loss layers. The *S* matrix of case II [$S^{(2)}$] gives the

positions of the ATRs of the system (i.e., its crossing points, where eigenvalues turn from unimodular to nonunimodular and vice versa are ATRs), which coincide with the peaks of the *g* factor, as discussed in the main text. Here, the transmission coefficients are on the diagonal as a result of a different criterion for *PT*-symmetric breaking phases [35]. $S^{(1)}$ and $S^{(2)}$ are defined as shown below:

$$\text{Case I}: \begin{pmatrix} b_- \\ c_+ \\ b_+ \\ c_- \end{pmatrix} = S^{(1)} \begin{pmatrix} a_+ \\ d_- \\ a_- \\ d_+ \end{pmatrix} \equiv \begin{pmatrix} r_{-+}^{(L)} & t_{--}^{(R)} & 0 & 0 \\ t_{++}^{(L)} & r_{+-}^{(R)} & 0 & 0 \\ 0 & 0 & r_{+-}^{(L)} & t_{++}^{(R)} \\ 0 & 0 & t_{--}^{(L)} & r_{-+}^{(R)} \end{pmatrix} \begin{pmatrix} a_+ \\ d_- \\ a_- \\ d_+ \end{pmatrix}, \tag{C1}$$

with two degenerate pairs of eigenvalues σ:

$$\sigma_{1,2}^{(1)} = \tfrac{1}{2}\{r^{(L)} + r^{(R)} \pm \sqrt{[r^{(L)} - r^{(R)}]^2 + 4t_{++}t_{--}}\}, \tag{C2}$$

$$\text{Case II}: \begin{pmatrix} c_+ \\ b_- \\ c_- \\ b_+ \end{pmatrix} = S^{(2)} \begin{pmatrix} a_+ \\ d_- \\ a_- \\ d_+ \end{pmatrix} \equiv \begin{pmatrix} t_{++}^{(L)} & r_{+-}^{(R)} & 0 & 0 \\ r_{-+}^{(L)} & t_{--}^{(R)} & 0 & 0 \\ 0 & 0 & t_{--}^{(L)} & r_{-+}^{(R)} \\ 0 & 0 & r_{+-}^{(L)} & t_{++}^{(R)} \end{pmatrix} \begin{pmatrix} a_+ \\ d_- \\ a_- \\ d_+ \end{pmatrix}, \tag{C3}$$

with two degenerate pairs of eigenvalues:

$$\sigma_{1,2}^{(2)} = \tfrac{1}{2}[t_{++} + t_{--} \pm \sqrt{(t_{--} - t_{++})^2 + 4r^{(L)}r^{(R)}}] \tag{C4}$$

APPENDIX D: SCATTERING PROPERTIES AND FURTHER EXAMPLES

To calculate the CD and *g* data shown in Figs. 2 and 4 of the main text, as well as the associated scattering matrix eigenvalues, one needs to evaluate transmission, reflection, and absorption for the corresponding systems. Here, we evaluate and present the reflection and transmission amplitudes as well as the total absorption $[A_+^{(L)} + A_-^{(L)}]$, $[A_+^{(R)} + A_-^{(R)}]$, and absorption difference [CD : $(A_+ - A_-)$—side independent] when RCP/+ and LCP/− waves impinge at the left and right side of the three-layer systems of Fig. 2 of the main text and another related system. Furthermore, we plot the eigenvalues of the scattering matrices $S^{(1)}$ and $S^{(2)}$ [Eqs. (C2) and (C4)] for the same systems. We calculate the above parameters for a range of frequencies much wider than that of Figs. 2 and 4 to illustrate that the high achievable values of the CD and *g* are not restricted to the range of Figs. 2 and 4 but are realizable in many different frequency ranges.

The first system considered is the one with *PT*-symmetric gain-loss layers (see Fig. 1 of the main text), with parameters those of Fig. 2(b), i.e., gain-loss slabs of thickness $d = 2.5 \ \mu$m and refractive index $n_{G/L} = 3 \mp 0.04i$, chiral layer of thickness $d = 10$ nm, chirality parameter $\kappa = \pm 5(10^{-4} + 10^{-5}i)$, and nonchiral refractive index $n_C = 1.33 + 0.01i$. In Fig. 8, left column and first panel, we show the transmission and reflection power coefficients for RCP and LCP waves incident from both sides of the system. In the second and third panels of Fig. 8, left column, we calculate the total absorption and the absorption difference (CD), respectively, in the same frequency range. We observe a broad frequency range where we have multiple regions with total

absorption close to zero; all these points coincide with peaks of the dissymmetry factor *g*. Regarding the absorption difference, the higher peaks here appear above the exceptional point (in the broken *PT* phase), where the scattering matrix eigenvalues of case I (see Appendix C) diverge (see fourth panel of Fig. 8, left column). These peaks indicate simultaneous coherent perfect absorption and lasing, which is one of the most exotic features of the *PT*-symmetric systems. Finally, in the last panel of Fig. 8, left column, we plot the scattering matrix $S^{(2)}$ eigenvalues (case II of the Appendix C), which give us the multiple positions of ATRs (points at which the eigenvalues turn from unimodular to nonunimodular and vice versa), where the absorption coefficients approach zero and maximization of *g* takes place.

The second system considered (see second/middle column of Fig. 8) is the general non-Hermitian system of Fig. 2(c) of the main text. Here, the gain layer has thickness $d = 2 \ \mu$m and refractive index $n_G = 2 - 0.05i$, the loss layer has thickness $d = 3 \ \mu$m and refractive index $n_L = 3 + 0.04i$, and the chiral layer has the same parameters as in the previous case (of the *PT*-symmetric gain-loss layers). The transmitted and reflected power for RCP and LCP waves incident from both system sides are illustrated in the middle column of Fig. 8, first panel. In the second and third panels, we show the total absorption and the absorption difference (CD), respectively, in the same frequency range. Comparing with the *PT*-symmetric case, we observe a similar behavior but a shift in frequency, due to the different gain-loss fraction. This illustrates the possibility to fully control the CD by tuning the gain-loss fraction; moreover, it indicates a flexibility and freedom in experimental realization and validation. The non-*PT* symmetry of the current system is also demonstrated by calculating the eigenvalues of scattering matrix $S^{(1)}$ (middle column, fourth panel), which are not unimodular in any frequency region.

The last system considered here has the same gain-loss configuration as in the previous case, but now the chiral layer is attached to the loss and not to the gain layer, as depicted
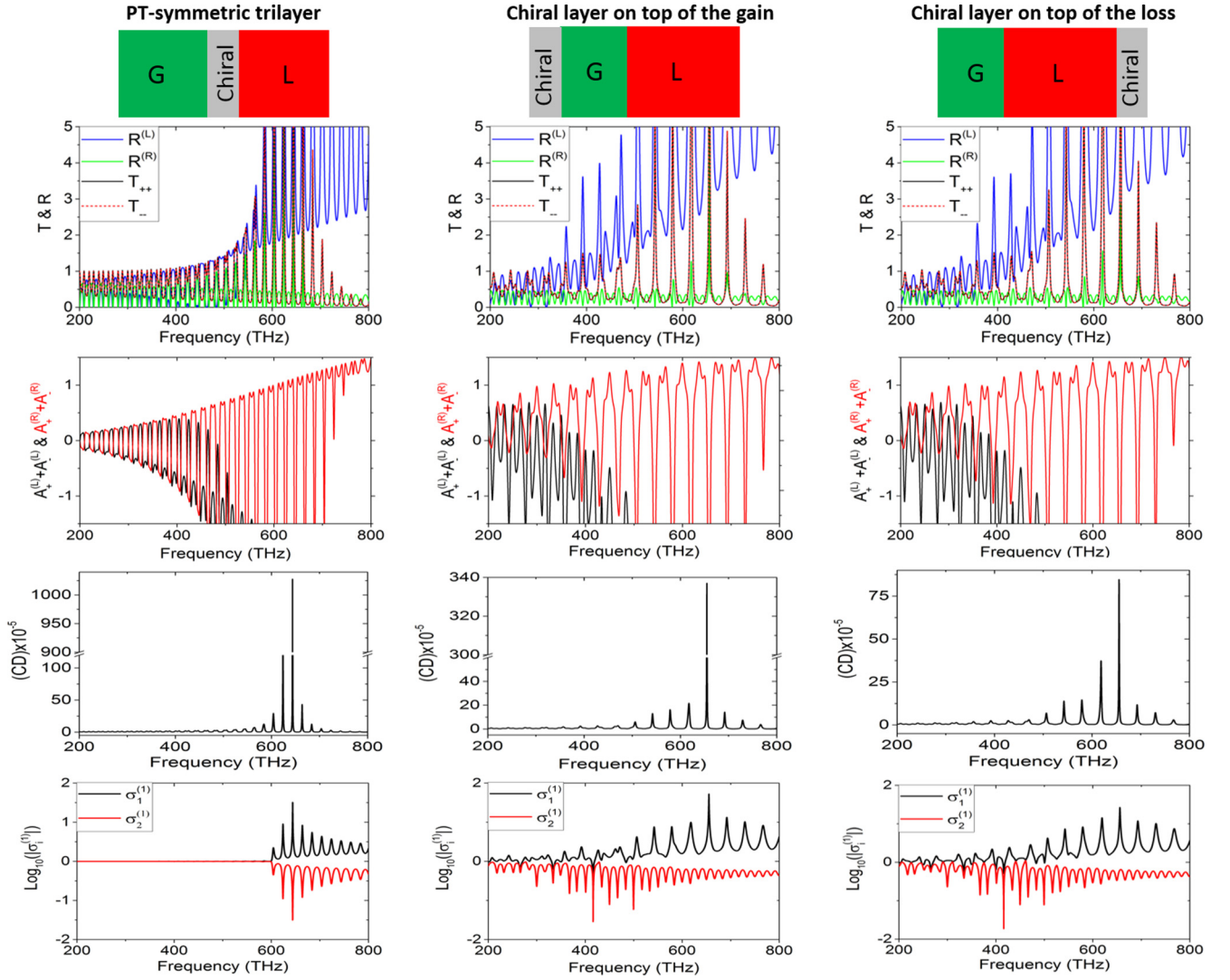
FIG. 8. Transmission and reflection power coefficients ($T_{ij} = |t_{ij}|^2$, $R_{ij} = |r_{ij}|^2$, respectively, $i,j = \{+,-\}$) (first row), total absorption ($A_+ + A_-$) (second row), absorption difference ($A_+ - A_-$) (third row), and scattering matrix eigenvalues (σ) for the scattering matrix $S^{(1)}$ (fourth row) and $S^{(2)}$ (fifth row), for right-handed circularly polarized (RCP/+) and left-handed circularly polarized (LCP/−) waves incident on the systems shown in the top insets from both the left and right side [the side is indicated by the superscripts (L) and (R), respectively]. Left column: system with *PT*-symmetric gain-loss layers; middle column: chiral-gain-loss general non-Hermitian system; right column: gain-loss-chiral non-Hermitian system. The material parameters and the layer thicknesses are mentioned in the text.

in the top inset of the right column of Fig. 8. Examining the transmission, reflection, and absorption results, we observe that the position of the resonances is practically the same as in the previous case (of middle column). However, there is quite a significant difference in the CD peak amplitudes, which is connected to the different chiral-loss impedance involved here compared with the chiral-gain one of the previous case and to the reflection asymmetry of the gain-loss bilayer, leading to different field amplitudes and thus different absorption in the chiral layer region.

APPENDIX E: STRONG CHIRAL DISSYMMETRY AT ACCIDENTAL FLUX-CONSERVING POINTS

A particularly interesting feature of *PT*-symmetric optical systems is the *accidental flux-conserving points*, correspond-

ing to $R^{(L)} = R^{(R)}$. If $T \leqslant 1$, it has been shown [35] that, at these points, the conservation relation $T + R = 1$ of the Hermitian systems holds, although the system is non-Hermitian, resulting in zero absorption. Thus, at such points, due to the vanishing of the total absorption, one can have high values of the dissymmetry factor even for very weak CD and for incidence from either side of the system. An even more intriguing feature of *PT* systems is the possibility of $R^{(L)} = R^{(R)} = 0$, $T = 1$, i.e., an accidental flux-conserving point coinciding with an ATR; such points are called points of *double accidental degeneracy* [35] and need special care for their engineering. At such points, the dissymmetry factor can be maximized in our three-layer *PT* systems. As an example, we calculate the dissymmetry factor for the system of Fig. 8 (left column) in a frequency region close to a point of quasidouble accidental degeneracy. The dissymmetry factor for CP waves incident
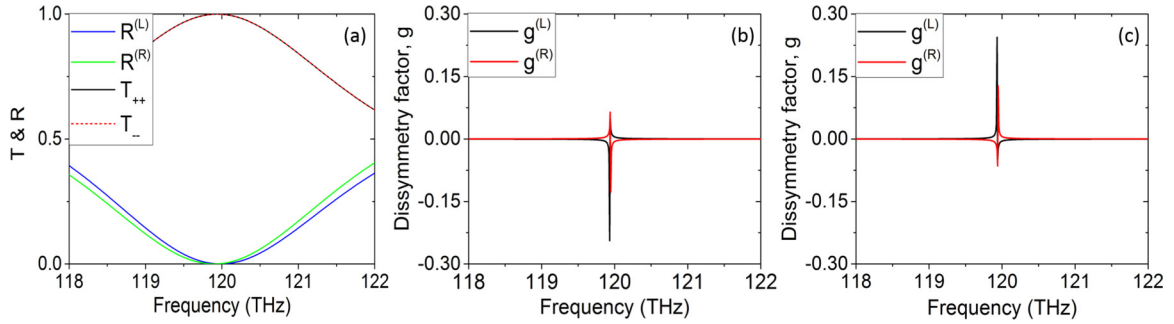
FIG. 9. (a) Transmission (T) and reflection (R) power coefficients for the system of Fig. 8—left-column; the dashed vertical line marks a point of quasi-double accidental degeneracy. (b) Dissymmetry factor (g) calculation for the system of (a) for chiral layer with $\kappa = +5(10^{-4} + 10^{-5}i)$. (c) The same as in (b) for $\kappa = -5(10^{-4} + 10^{-5}i)$. The black lines correspond to waves incident from the left side of the system [marked by the superscript (L)] and the red lines from the right side [marked by the superscript (R)]. The subscripts $+/-$ indicate right/left circularly polarized waves.

from both sides and for positive/negative chirality parameters are depicted in Figs. 9(b) and 9(c). We observe strong dissymmetry factors $g^{(L)} \cong 0.24$ and $g^{(R)} \cong 0.12$ (one order of magnitude larger than the dissymmetry factors of Fig. 4) at frequency ~ 119.8 THz, which is a point of quasidouble accidental degeneracy, as shown in Fig. 9(a) (we note again here

that the presence of the chiral layer perturbs the *PT*-symmetric character of the gain-loss layers, making the three-layer system not fully *PT* symmetric). In closing, we should note that the frequency region ~ 119.8 THz is not the only region where accidental flux conservation occurs in our system; there are multiple points/regions with this property [35].

APPENDIX F: ABSORPTION, CD, AND DISYMMETRY FACTOR FOR A THIN CHIRAL LAYER—DERIVATION OF EQ. (1)

We start with Maxwell's equations and the constitutive relations for a (Pasteur) chiral medium:

$$\nabla \times \mathbf{E}(\mathbf{r}, t) = -\frac{\partial \mathbf{B}(\mathbf{r}, t)}{dt}, \tag{F1}$$

$$\nabla \times \mathbf{H}(\mathbf{r}, t) = \frac{\partial \mathbf{D}(\mathbf{r}, t)}{dt}, \tag{F2}$$

$$\mathbf{D}(\mathbf{r}, t) = \varepsilon \mathbf{E}(\mathbf{r}, t) + \frac{i\kappa}{c} \mathbf{H}(\mathbf{r}, t), \tag{F3}$$

$$\mathbf{B}(\mathbf{r}, t) = \mu \mathbf{H}(\mathbf{r}, t) - \frac{i\kappa}{c} \mathbf{E}(\mathbf{r}, t), \tag{F4}$$

where $\varepsilon = \varepsilon_r \varepsilon_0$ and $\mu = \mu_r \mu_0$ are the electric permittivity and magnetic permeability, respectively, and κ is the (Pasteur) chirality parameter. From classical electrodynamics, we know that electromagnetic power density (P) is defined as the flux of Poynting's vector $\mathbf{S}(\mathbf{r}, t)$, which describes the flow of energy per unit time per unit area (J/sm^2 in SI units). For complex time-harmonic electromagnetic fields of the form $e^{-i\omega t}$, the time averaged P (over a period T) can be written as

$$\langle P \rangle_T = [\nabla \cdot \mathbf{S}(\mathbf{r})] = \tfrac{1}{2} \mathrm{Re}\{\nabla \cdot [\mathbf{E}(\mathbf{r}) \times \mathbf{H}^*(\mathbf{r})]\}. \tag{F5}$$

Inserting Maxwell's Eqs. (F1) and (F2) into the expression $\nabla \cdot [\mathbf{E}(\mathbf{r}, t) \times \mathbf{H}^*(\mathbf{r}, t)]$, considering the vector identity $\nabla \cdot (\mathbf{A} \times \mathbf{B}) = \mathbf{B} \cdot (\nabla \times \mathbf{A}) - \mathbf{A} \cdot (\nabla \times \mathbf{B})$ and assuming $\varepsilon = \varepsilon' + i\varepsilon''$, $\mu = \mu' + i\mu''$, and $\kappa = \kappa' + i\kappa''$, we can write

$$[\mathbf{H}^* \cdot (\nabla \times \mathbf{E}) - \mathbf{E} \cdot (\nabla \times \mathbf{H}^*)] = \left[\mathbf{H}^* \cdot \left(-\frac{\partial \mathbf{B}}{dt}\right) - \mathbf{E} \cdot \left(\frac{\partial \mathbf{D}^*}{dt}\right)\right]$$

$$= [\mathbf{H}^* \cdot (i\omega \mathbf{B}) - \mathbf{E} \cdot (i\omega \mathbf{D}^*)] = [-i\omega(\mathbf{E} \cdot \mathbf{D}^* - \beta \cdot \mathbf{H}^*)]$$

$$= -i\omega \left[\mathbf{E} \cdot \left(\varepsilon^* \mathbf{E}^* - \frac{i\kappa^*}{c} \mathbf{H}^*\right) - \left(\mu \mathbf{H} - \frac{i\kappa}{c} \mathbf{E}\right) \cdot \mathbf{H}^*\right]$$

$$= -i\omega \left[\varepsilon^* |\mathbf{E}|^2 - \mu |\mathbf{H}|^2 + \frac{i(\kappa - \kappa^*)}{c} \mathbf{E} \cdot \mathbf{H}^*\right]$$

$$= -i\omega \left\{(\varepsilon' - i\varepsilon'')|\mathbf{E}|^2 - (\mu' + i\mu'')|\mathbf{H}|^2 - \frac{2\kappa''}{c}[\mathrm{Re}(\mathbf{E} \cdot \mathbf{H}^*) + i\mathrm{Im}(\mathbf{E} \cdot \mathbf{H}^*)]\right\}. \tag{F6}$$

Therefore, from Eqs. (F5) and (F6), we can write

$$\langle P \rangle_T = -\frac{\omega}{2}\left[\varepsilon''|\mathrm{E}|^2 + \mu''|\mathbf{H}|^2 - \frac{2\kappa''}{c}\mathrm{Im}(\mathbf{E}\cdot\mathbf{H}^*)\right]. \tag{F7}$$

Defining optical chirality [7] as

$$C = -\frac{\omega}{2c^2}\mathrm{Im}(\mathbf{E}\cdot\mathbf{H}^*), \tag{F8}$$

Eq. (F7) becomes

$$\langle P \rangle_T = -\frac{\omega}{2}(\varepsilon''|\mathrm{E}|^2 + \mu''|\mathbf{H}|^2) + 2c\kappa''C. \tag{F9}$$

For loss media $\mathrm{Re}[\nabla\mathbf{S}(\mathbf{r},t)] < 0$; hence, the absorbed power can be computed by integrating the time-averaged power density, Eq. (F9), over the entire volume of the chiral layer. Assuming RCP/+ or LCP/− waves, we can write

$$A_\pm = \int\left[\frac{\omega}{2}(\varepsilon''|\mathrm{E}_\pm|^2 + \mu''|\mathbf{H}_\pm|^2) + 2c\kappa''C_\pm\right]dV. \tag{F10}$$

In the case in which the chiral layer is very thin ($k_\pm d \ll 1$) or the chirality (κ) is very weak, then $|\mathrm{E}_+|^2 \approx |\mathbf{E}_-|^2 \cong |\mathbf{E}|^2$, $|\mathbf{H}_+|^2 \approx |\mathbf{H}_-|^2 \cong |\mathbf{H}|^2$, and $C_+ = -C_- \cong C$. Then the CD, defined as $= A_+ - A_-$, becomes

$$\mathrm{CD} = 2c\kappa''\int(C_+ - C_-)dV = 4c\kappa'' \int C\,dV, \tag{F11}$$

and the total absorption of the system as

$$A_+ + A_- = \omega\,\varepsilon''\int|\mathbf{E}|^2 dV + \omega\mu''\int|\mathbf{H}|^2 dV + 4c\kappa''\int C\,dV, \tag{F12}$$

Combining Eqs. (F11) and (F12), we can calculate the dissymmetry factor g as the following:

$$g = \frac{2\mathrm{CD}}{A_+ + A_-} = \frac{8c\kappa''\int \mathbf{C}\,dV}{\omega(\varepsilon''\int[|\mathbf{E}|^2]\,dV + \mu''\int[|\mathbf{H}|^2]\,dV\,)}. \tag{F13}$$

[1] C. Caloz and A. Sihvola, IEEE Antennas Propag. Mag. **62**, 58 (2020).

[2] S. Capozziello and A. Lattanzi, Chirality **18**, 17 (2006).

[3] L. A. Nguyen, H. He, and C. Pham-Huy, Int. J. Biomed. Sci. **2**, 85 (2006).

[4] P. L. Polavarapu (ed.), *Chiral Analysis: Advances in Spectroscopy, Chromatography and Emerging Methods*, 2nd Ed. (Elsevier, Amsterdam, 2018).

[5] M. A. Bouchiat and C. Bouchiat, Rep. Prog. Phys. **60**, 1351 (1997).

[6] J. Mun, M. Kim, Y. Yang, T. Badloe, J. Ni, Y. Chen, C.-W. Qiu, and J. Rho, Light Sci. Appl. **9**, 139 (2020).

[7] Y. Tang and A. E. Cohen, Phys. Rev. Lett. **104**, 163901 (2010).

[8] J.-B. Biot, Mem. Acad. Sci. **2**, 41 (1817).

[9] E. Mohammadi, A. Tavakoli, P. Dehkhoda, Y. Jahani, K. L. Tsakmakidis, A. Tittl, and H. Altug, ACS Photonics **6**, 1939 (2019).

[10] E. Mohammadi, K. L. Tsakmakidis, A. Askarpour, P. Dehkhoda, A. Tavakoli, and H. Altug, ACS Photonics **5**, 2669 (2018).

[11] Y. Zhao, A. A. E. Saleh, and J. A. Dionne, ACS Photonics **3**, 304 (2016).

[12] M. Schaferling, X. Yin, N. Engheta, and H. Giessen, ACS Photonics **1**, 530 (2014).

[13] F. Graf, J. Feis, X. Garcia-Santiago, M. Wegener, C. Rockstuhl, and I. Fernandez-Corbaton, ACS Photonics **6**, 482 (2019).

[14] M. L. Solomon, J. Hu, M. Lawrence, A. García-Etxarri, and J. A. Dionne, ACS Photonics **6**, 43 (2019).

[15] Y. Zhao, A. N. Askarpour, L. Sun, J. Shi, X. Li, and A. Alù, Nat. Comm. **8**, 14180 (2017).

[16] S. Droulias and L. Bougas, ACS Photonics **6**, 1485 (2019).

[17] S. Droulias and L. Bougas, Nano Lett. **20**, 5960 (2020).

[18] C. S. Ho, A. Garcia-Etxarri, Y. Zhao, and J. Dionne, ACS Photonics **4**, 197 (2017).

[19] E. Mohammadi, A. Tittl, K. L. Tsakmakidis, T. V. Raziman, and A. G. Curto, ACS Photonics **8**, 1754 (2021).

[20] J. Feis, D. Beutel, J. Köpfler, X. Garcia-Santiago, C. Rockstuhl, M. Wegener, and I. Fernandez-Corbaton, Phys. Rev. Lett. **124**, 033201 (2020).

[21] T. J. Davis and E. Hendry, Phys. Rev. B **87**, 085405 (2013).

[22] D. Sofikitis, L. Bougas, G. E. Katsoprinakis, A. K. Spiliotis, B. Loppinet, and T. P. Rakitzis, Nature (London) **514**, 76 (2014).

[23] P. Scott, X. Garcia-Santiago, D. Beutel, C. Rockstuhl, M. Wegener, and I. Fernandez-Corbaton, Appl. Phys. Rev. **7**, 041413 (2020).

[24] T. Muller, K. B. Wiberg, and P. H. Vaccaro, J. Phys. Chem. A **104**, 5959 (2000).

[25] L. V. Poulikakos, P. Gutsche, K. M. McPeak, S. Burger, J. Niegemann, C. Hafner, and D. J. Norris, ACS Photonics **3**, 1619 (2016).

[26] U. Kilic, M. Hilfiker, A. Ruder, R. Feder, E. Schubert, M. Schubert, and C. Argyropoulos, Adv. Funct. Mater. **31**, 2010329 (2021).

[27] S. Droulias, Phys. Rev. B **102**, 075119 (2020).

[28] M. Hanifeh, M. Albooyeh, and F. Capolino, ACS Photonics **7**, 2682 (2020).

[29] J. L. Greenfield, J. Wade, J. R. Brandt, X. Shi, T. J. Penfoldd, and M. J. Fuchter, Chem. Sci. **12**, 8589 (2021).

[30] W. Kuhn, Trans. Faraday Soc. **26**, 293 (1930).

[31] M. Schäferling, D. Dregely, M. Hantschel, and H. Giessen, Phys. Rev. X **2**, 031010 (2012).

[32] M. L. Solomon, A. A. E. Saleh, L. V. Poulikakos, J. M. Abendroth, L. F. Tadesse, and J. A. Dionne, Acc. Chem. Res. **53**, 588 (2020).

[33] K. A. Forbes and D. L. Andrews, Phys. Rev. A **99**, 023837 (2019).

[34] J. T. Collins, K. R. Rusimova, D. C. Hooper, H.-H. Jeong, L. Ohnoutek, F. Pradaux-Caggiano, T. Verbiest, D. R. Carbery, P. Fischer, and V. K. Valev, Phys. Rev. X **9**, 011024 (2019).

[35] Li Ge, Y. D. Chong, and A. D. Stone, Phys. Rev. A **85**, 023802 (2012).

[36] S. Savoia, G. Castaldi, V. Galdi, A. Alù, and N. Engheta, Phys. Rev. B **89**, 085105 (2014).

[37] W. Chen, ¸S. K. Özdemir, G. Zhao, J. Wiersig, and L. Yang, Nature (London) **548**, 192 (2017).

[38] Q. Zhong, J. Ren, M. Khajavikhan, D. N. Christodoulides, S. K. Özdemir, and R. El-Ganainy, Phys. Rev. Lett. **122**, 153902 (2019).

[39] S. Yu, X. Piao, and N. Park, Sci. Rep. **6**, 37754 (2020).

[40] S. Hou, T. Wu, W. Zhang, and X. Zhang, J. Phys. Chem. C **124**, 24970 (2020).

[41] A. Guo, G. J. Salamo, D. Duchesne, R. Morandotti, M. Volatier-Ravat, V. Aimez, G. A. Siviloglou, and D. N. Christodoulides, Phys. Rev. Lett. **103**, 093902 (2009).

[42] C. E. Ruter, K. G. Makris, R. El-Ganainy, D. N. Christodoulides, M. Sagev, and D. Kip, Nat. Phys. **6**, 192 (2010).

[43] L. Feng, M. Ayache, J. Huang, Y. Xu, M. Lu, Y. Chen, Y. Fainman, and A. Scherer, Science **333**, 729 (2011).

[44] S. Droulias, I. Katsantonis, M. Kafesaki, C. M. Soukoulis, and E. N. Economou, Phys. Rev. B **100**, 205133 (2019).

[45] K. G. Makris, R. El-Ganainy, D. N. Christodoulides, and Z. H. Musslimani, Phys. Rev. Lett. **100**, 103904 (2008).

[46] Z. Lin, H. Ramezani, T. Eichelkraut, T. Kottos, H. Cao, and D. N. Christodoulides, Phys. Rev. Lett. **106**, 213901 (2011).

[47] Y. D. Chong, Li. Ge, and A. D. Stone, Phys. Rev. Lett. **106**, 093902 (2011).

[48] R. El-Ganainy, K. G. Makris, D. N. Christodoulides, and Z. H. Musslimani, Opt. Lett. **32**, 2632 (2007).

[49] L. Ge and L. Feng, Phys. Rev. A. **94**, 043836 (2016).

[50] S. Droulias, I. Katsantonis, M. Kafesaki, C. M. Soukoulis, and E. N. Economou, Phys. Rev. Lett **122**, 213201 (2019).

[51] I. Katsantonis, S. Droulias, C. M. Soukoulis, E. N. Economou, and M. Kafesaki, Phys. Rev. B **101**, 214109 (2020).

[52] I. Katsantonis, S. Droulias, C. M. Soukoulis, E. N. Economou, and M. Kafesaki, Photonics **7**, 43 (2020).

[53] A. Krasnok, N. Nefedkin, and A. Alù, IEEE Antennas and Propagation Magazine, **63**, 110 (2021).

[54] E. U. Condon, Rev. Mod. Phys. **9**, 432 (1937).

[55] V. I. V. Lindell, A. H. Sihvola, S. A. Tretyakov, and A. J. Viitanen, *Electromagnetic Waves in Chiral and Bi-Isotropic Media* (Artech House Publishers, Boston, 1994).

[56] B. Wang, J. Zhou, T. Koschny, M. Kafesaki, and C. M. Soukoulis, J. Opt. A **11**, 114003 (2009).

[57] J. Garcia-Guirado, M. Svedendahl, J. Puigdollers, and R. Quidant, Nano Lett. **20**, 585 (2020).

[58] Z. J. Wong, Y.-L. Xu, J. Kim, K. OBrien, Y. Wang, L. Feng, and X. Zhang, Nat. Photonics **10**, 796 (2016).

[59] A. Krasnok and A. Alù, Proc. IEEE **108**, 628, (2020).

[60] X. Piao, S. Yu, J. Hong, and N. Park, Sci. Rep. **5**, 16585 (2015).

[61] S. Wuestner, A. Pusch, K. L. Tsakmakidis, J. M. Hamm, and O. Hess, Phys. Rev. Lett. **105**, 127401 (2010).

[62] V. I. Klimov, A. A. Michailovsky, S. Xu, A. Malko, J. A. Hollingsworth, C. A. Leatherdale, H. J. Eisler, and M. G. Bawendi, Science **290**, 314 (2000).

[63] F. Lohof, A. Steinhoff, M. Florian, M. Lorke, D. Erben, F. Jahnke, and C. Gies, Nano Lett. **19**, 210 (2019).

[64] S. Droulias, A. Jain, T. Koschny, and C. M. Soukoulis, Phys. Rev. B **96**, 155143 (2017).

[65] L. Bsawmaii, E. Gamet, F. Royer, S. Neveu, and D. Jamon, Opt. Express **28**, 8436 (2020).

[66] X. Zhang, G. Yu, G. Yuan, and Y. Lv, Opt. Mater. **114**, 110771 (2021).

[67] P. Markos and C. M. Soukoulis, *Wave Propagation: From Electrons to Photonic Crystals and Left-Handed Materials* (Princeton University Press, Princeton, 2008).

[68] J. Lekner, Pure Appl. Opt. **5**, 417 (1996).

[69] C. M. Bender, Rep. Prog. Phys. **70**, 947 (2007).